



# An ALMA Survey of $\lambda$ Orionis Disks: From Supernovae to Planet Formation

Megan Ansdell<sup>1,2</sup>, Thomas J. Haworth<sup>3</sup>, Jonathan P. Williams<sup>4</sup>, Stefano Facchini<sup>5</sup>, Andrew Winter<sup>6</sup>, Carlo F. Manara<sup>5</sup>, Alvaro Hacar<sup>7</sup>, Eugene Chiang<sup>8</sup>, Sierk van Terwisga<sup>9</sup>, Nienke van der Marel<sup>10</sup>, and Ewine F. van Dishoeck<sup>7</sup>

<sup>1</sup> Flatiron Institute, Simons Foundation, 162 Fifth Ave., New York, NY 10010, USA; [megan.c.ansdell@nasa.gov](mailto:megan.c.ansdell@nasa.gov)

<sup>2</sup> NASA Headquarters, 300 E Street SW, Washington, DC 20546, USA

<sup>3</sup> Astronomy Unit, School of Physics and Astronomy, Queen Mary University of London, London E1 4NS, UK

<sup>4</sup> Institute for Astronomy, University of Hawai'i at Mānoa, Honolulu, HI, USA

<sup>5</sup> European Southern Observatory, Karl-Schwarzschild-Str. 2, D-85748 Garching bei München, Germany

<sup>6</sup> Astronomisches Rechen-Institut, Zentrum für Astronomie der Universität Heidelberg, Mönchhofstraße 12-14, D-69120 Heidelberg, Germany

<sup>7</sup> Leiden Observatory, Leiden University, P.O. Box 9513, 2300-RA Leiden, The Netherlands

<sup>8</sup> Department of Astronomy, University of California at Berkeley, Berkeley, CA 94720, USA

<sup>9</sup> Max-Planck-Institute for Astronomy, Königstuhl 17, D-69117 Heidelberg, Germany

<sup>10</sup> Department of Physics & Astronomy, University of Victoria, Victoria, BC, V8P 1A1, Canada

Received 2020 May 7; revised 2020 August 28; accepted 2020 September 16; published 2020 November 6

## Abstract

Protoplanetary disk surveys by the Atacama Large Millimeter/submillimeter Array (ALMA) are now probing a range of environmental conditions, from low-mass star-forming regions like Lupus to massive OB clusters like  $\sigma$  Orionis. Here we conduct an ALMA survey of protoplanetary disks in  $\lambda$  Orionis, an  $\sim 5$  Myr old OB cluster in Orion with dust mass sensitivities comparable to the surveys of nearby regions ( $\sim 0.4 M_{\oplus}$ ). We assess how massive OB stars impact planet formation, in particular from the supernova that may have occurred  $\sim 1$  Myr ago in the core of  $\lambda$  Orionis; studying these effects is important, as most planetary systems, including our solar system, are likely born in cluster environments. We find that the effects of massive stars, in the form of presupernova feedback and/or a supernova itself, do not appear to significantly reduce the available planet-forming material otherwise expected at this evolved age. We also compare a lingering massive “outlier” disk in  $\lambda$  Orionis to similar systems in other evolved regions, hypothesizing that these outliers host companions in their inner disks that suppress disk dispersal to extend the lifetimes of their outer primordial disks. We conclude with numerous avenues for future work that highlight how  $\lambda$  Orionis still has much to teach us about perhaps one of the most common types of planet-forming environments in the Galaxy.

*Unified Astronomy Thesaurus concepts:* [Protoplanetary disks \(1300\)](#); [Circumstellar disks \(235\)](#); [Millimeter astronomy \(1061\)](#); [Planet formation \(1241\)](#); [Exoplanet formation \(492\)](#); [Submillimeter astronomy \(1647\)](#); [OB stars \(1141\)](#); [Supernovae \(1668\)](#); [Surveys \(1671\)](#)

## 1. Introduction

Thousands of diverse exoplanetary systems have now been discovered (e.g., see review in Winn & Fabrycky 2015), yet how they all formed remains unclear due to our still-incomplete understanding of the evolution of the progenitor protoplanetary disks. These disks are traditionally thought to evolve through viscous accretion (e.g., Lynden-Bell & Pringle 1974), where turbulence redistributes angular momentum and drives material onto the central star. However, other processes, both internal and external to the disks, can also significantly influence their evolution. In particular, the external influence of massive OB stars on the disks of surrounding lower-mass stars is important to study, as many planetary systems, including our solar system, are likely born in cluster environments (e.g., Adams 2010; Winter et al. 2020).

In stellar clusters, the ultraviolet (UV) emission from the OB stars induces thermal winds from nearby disks, which effectively remove planet-forming material from their outer regions in a process called “external photoevaporation” (e.g., Hollenbach et al. 1994). Theoretical work suggests that external photoevaporation can severely shorten disk lifetimes and truncate outer disk radii in cluster environments, whereas stellar encounters play a relatively insignificant role in sculpting disk populations (e.g., Scally & Clarke 2001; Concha-Ramírez et al. 2019), even in moderate UV environments (e.g., Facchini et al. 2016; Haworth et al. 2018; Winter et al. 2018). Moreover, external photoevaporation of the outer disk is theorized to dominate over viscous spreading under

realistic cluster conditions and dust grain growth prescriptions (e.g., Clarke 2007; Facchini et al. 2016; Winter et al. 2018). While direct detection of photoevaporative disk winds is observationally challenging, a handful of cases exist (e.g., Henney & O’Dell 1999; Rigliaco et al. 2009). Meanwhile, indirect evidence of external photoevaporation from observations of its expected impact on other disk properties is growing (e.g., Mann et al. 2014; Guarcello et al. 2016; Kim et al. 2016; Ansdell et al. 2017; van Terwisga et al. 2019b).

Still, our understanding of how disk evolution is altered when one of these rapidly evolving OB stars inevitably goes supernova remains limited, due in part to the lack of recent supernova events in nearby star-forming regions (SFRs) available for study. This makes the  $\lambda$  Orionis cluster a key target, as a supernova is thought to have occurred in the core of the region  $\sim 1$  Myr ago (e.g., Cunha & Smith 1996; Dolan & Mathieu 2001). At  $\sim 5$  Myr of age (e.g., Hernández et al. 2009),  $\lambda$  Orionis may therefore provide a rare snapshot of an evolved SFR post-supernova, with the remaining OB stars, lower-mass stellar population, and remnant molecular cloud all still present. Supernovae are theorized to strip significant amounts of mass from disks around nearby stars via ram pressure (e.g., Close & Pittard 2017), as well as expose them to enhanced cosmic-ray ionization rates that accelerate carbon processing of CO into other molecules (e.g., Eistrup et al. 2016; Bosman et al. 2018; Schwarz et al. 2018), thereby providing predictions to test against observations.

A partial survey of the disk population in  $\lambda$  Orionis was conducted at millimeter wavelengths by Ansdell et al. (2015) with SCUBA-2 on the James Clerk Maxwell Telescope (JCMT/SCUBA-2). Observations of disks at these longer wavelengths are particularly useful because any optically thin continuum emission can be related to the available planet-forming solids in the disk (e.g., Hildebrand 1983; Andrews 2015), while various molecular lines can probe gas content and/or chemistry (e.g., Miotello et al. 2017, 2019; van Terwisga et al. 2019b; Booth & Ilee 2020). However, due to the evolved age ( $\sim 5$  Myr) and large distance ( $\sim 1400$  pc) of  $\lambda$  Orionis, combined with the limited sensitivity of JCMT/SCUBA-2, Ansdell et al. (2015) detected only one disk in their survey. Fortunately, the Atacama Large Millimeter/submillimeter Array (ALMA) now provides the high sensitivity required to efficiently survey the disk population in  $\lambda$  Orionis to dust mass sensitivities that are commonly achieved for nearby ( $\sim 150$  pc) SFRs like Lupus (Ansdell et al. 2016, 2018), Chamaeleon I (Pascucci et al. 2016),  $\rho$  Ophiuchus (Cieza et al. 2019), and Upper Sco (Barenfeld et al. 2016). This paper presents the results of such an ALMA survey.

We begin in Section 2 by discussing the formation and evolution of  $\lambda$  Orionis, as the cluster’s history is central to our analysis. In Section 3, we describe our sample of protoplanetary disks and their host star properties. Our ALMA survey of these disks and the key observational results are presented in Section 4, while the basic disk properties are derived in Section 5. We then examine the implications for our understanding of how OB stars affect disk evolution in Section 6, which also discusses how massive “outlier” disks in evolved regions like  $\lambda$  Orionis may improve our knowledge of the pathways of planet formation and disk dispersal. We summarize our findings and provide avenues for future work in Section 7.

## 2. The $\lambda$ Orionis Cluster

The formation, evolution, and current state of the  $\lambda$  Orionis cluster have been studied and debated in many works (e.g., Maddalena & Morris 1987; Cunha & Smith 1996; Dolan & Mathieu 2001; Hernández et al. 2009; Bayo et al. 2011; Mathieu 2015; Kounkel et al. 2018). In this section, we briefly summarize the existing observations of the cluster, then assume a commonly adopted but still debated interpretation that has implications for our later analysis.

As illustrated in Figure 1,  $\lambda$  Orionis currently consists of several hundred low-mass members centered on a core of OB stars. The most massive is the O8III star  $\lambda$  Ori, the brightest in the head of the Orion constellation. Although  $\lambda$  Ori is the only O-type star in the cluster, it has a B0V companion at 1900 au projected separation, and this binary system is accompanied by nine other B-type stars (some close binaries themselves) in a dense  $\sim 2$  pc radius clump in the cluster center (Murdin & Penston 1977). The interstellar dust and molecular gas in the region are largely confined to an  $\sim 30$  pc radius ring (or possibly shell; Lee et al. 2015) that is centered on the clump of OB stars, encompasses the lower-mass population, and is rapidly expanding at  $\sim 14$  km s $^{-1}$  (e.g., Maddalena & Morris 1987; Lang et al. 2000). As shown in Figure 1, many of the  $\lambda$  Orionis members also have proper motions directed radially away from the cluster center, with the more distant stars moving away the fastest (Kounkel et al. 2018).

The age of the lower-mass stellar population in  $\lambda$  Orionis is  $\sim 5$  Myr (e.g., Dolan & Mathieu 2001; Hernández et al. 2009). This is largely based on Strömgren photometry of the most massive OB stars, which suggests that their formation occurred

$\sim 6$  Myr ago, combined with photometric and spectroscopic surveys of the surrounding pre-main-sequence stars, which indicate an epoch of lower-mass star formation that began soon after but was halted  $\sim 1$ – $2$  Myr ago (Dolan & Mathieu 1999, 2001). In this work, we do not consider the younger dark Barnard 30 and Barnard 35 clouds, located along the edge of the ring, as part of the  $\lambda$  Orionis cluster.

We adopt the common interpretation in the literature of these observations, which is that an O-type star exploded as a supernova  $\sim 1$  Myr ago in the cluster core, carving out the central cloud to create the molecular ring/shell, while terminating star formation in the region (Cunha & Smith 1996; Dolan & Mathieu 1999, 2001; Mathieu 2008, 2015). However, we note that presupernova feedback may also carve out central cavities in molecular clouds (e.g., Dale et al. 2014). Moreover, although the radial motions of the  $\lambda$  Orionis members have been attributed to a “single-trigger” expansion caused by the supernova (Kounkel et al. 2018), such kinematics can result from any mechanism that removes the interstellar gas and its gravitational potential (Winter et al. 2019), and outward acceleration may even be aided by gravitational feedback of the dispersed gas (Zamora-Avilés et al. 2019). While these and other caveats are discussed further in Section 6.1, the massive stars in  $\lambda$  Orionis, whether through presupernova feedback and/or a supernova event itself, have played a key role in shaping the region.

## 3. Sample

### 3.1. Disk Sample Selection

Like most SFRs, the disk census in  $\lambda$  Orionis is based on targeted Spitzer observations, which can identify stars exhibiting excess emission above the stellar photosphere at near-infrared (IRAC 3.6, 4.5, 5.8, and 8.0  $\mu$ m; Fazio et al. 2004) and/or mid-infrared (MIPS 24  $\mu$ m; Rieke et al. 2004) wavelengths, where dust emits efficiently. Hernández et al. (2009) used Spitzer data to study the intermediate-mass population in  $\lambda$  Orionis, finding 29 members earlier than F5 but only 10 bearing disks. They classified the nine sources with moderate infrared excess as debris disks and the one source with large infrared excess as an optically thick disk. Hernández et al. (2010) then studied the lower-mass population in  $\lambda$  Orionis, finding 436 members down to the substellar limit but only 49 with disks. They grouped these disks according to their spectral energy distributions (SEDs)—optically thick disks had the largest excesses, evolved disks had smaller excesses, and (pre)transition disks exhibited signs of inner disk clearings. We exclude from our sample the nine debris disks, as these are likely second-generation dust disks (Wyatt 2008), resulting in an initial sample of 50 primordial (or protoplanetary) disks. We use the same naming conventions as Hernández et al. (2009, 2010) in this work.

As shown in Figure 1, the region surveyed by Spitzer (white box) only covers  $\sim 3$  pc from the cluster center. Recent kinematic studies of the Orion Complex using astrometric data from Gaia (Gaia Collaboration et al. 2016) Data Release 2 (DR2; Gaia Collaboration et al. 2018) combined with spectroscopic data from the Apache Point Observatory Galactic Evolution Experiment (APOGEE; Majewski et al. 2017) revealed a population of radially expanding  $\lambda$  Orionis members that extend well beyond this area (Kounkel et al. 2018). Surveys for disks in these outer regions have not yet been

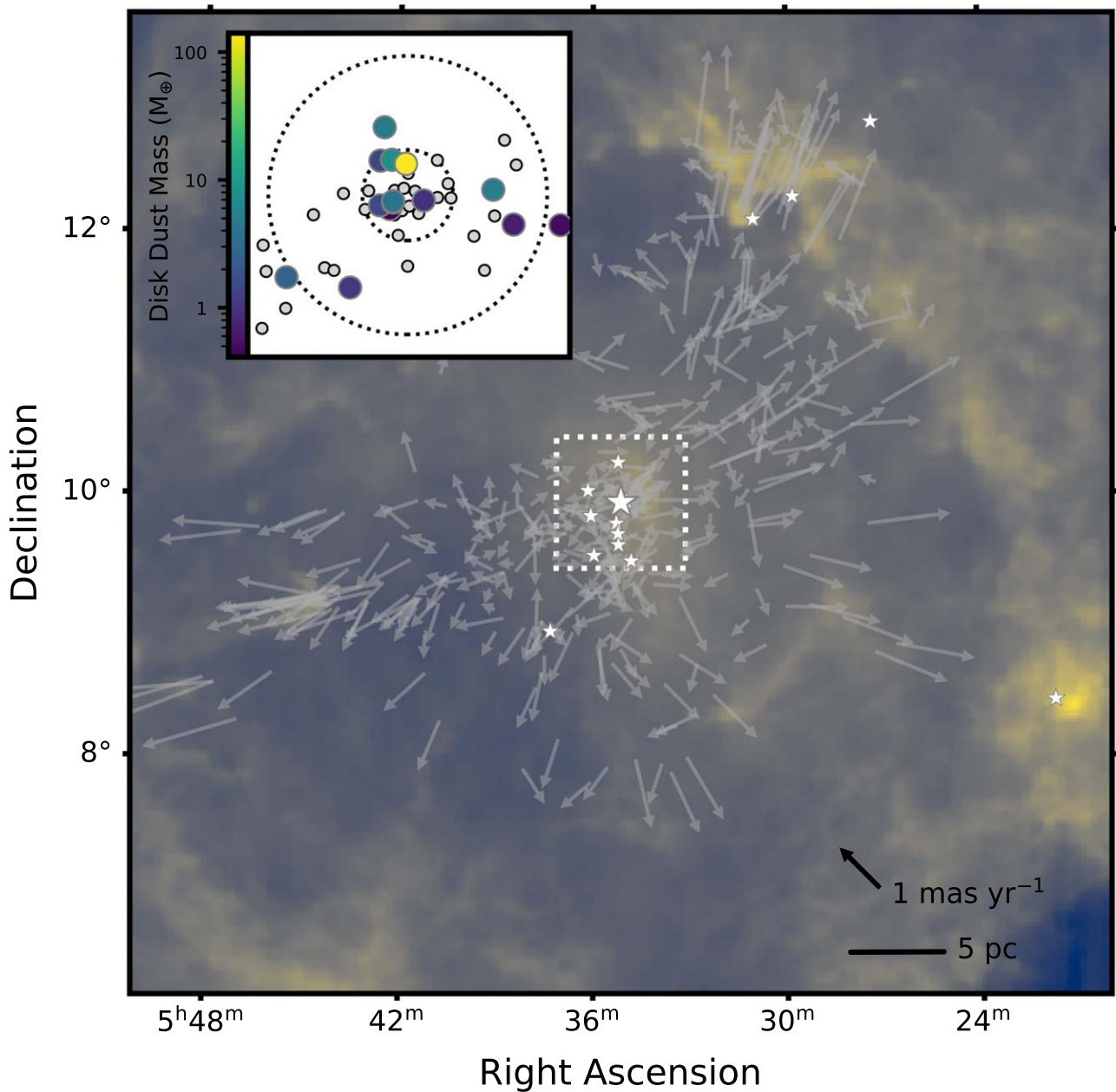


**Figure 1.** An IRAS  $100\ \mu\text{m}$  image of the  $\lambda$  Orionis cluster. The white dashed box outlines the region surveyed for disks with Spitzer in Hernández et al. (2009, 2010), which we use as the basis of our ALMA survey sample selection (Section 3.1). The inset zooms in on this region. The large circles are our ALMA detections color-coded by dust mass (Section 5.1), while the small gray circles are the nondetections (Section 4.2); the dotted lines represent 1 and 3 pc radial distances from the  $\lambda$  Ori system at the center of the cluster. Gray arrows show the Gaia DR2 proper motions of the cluster members identified by Kounkel et al. (2018) in the LSR frame with the median cluster value subtracted; a reference vector of magnitude  $1\ \text{mas yr}^{-1}$  and a scale bar of 5 pc are shown in the lower right corner. The small white stars are the locations of the B-type stars in the region, and the larger white star is the location of the  $\lambda$  Ori system, which contains the only O-type star in the region (Section 2).

conducted, making it possible that our ALMA sample based solely on Spitzer data is incomplete. Nevertheless, the low protoplanetary disk fraction in  $\lambda$  Orionis inferred from the Spitzer data is consistent with the  $\sim 5$  Myr age of the cluster, as it follows the well-known exponential decline in disk frequency with age (e.g., see Figure 14 in Hernández et al. 2007). Moreover, the issue of a potentially incomplete disk census when using targeted Spitzer observations for the sample selection is a general (albeit moderate) problem facing the ALMA disk demographic literature, as Gaia continues to reveal missed or interloping stellar populations in young SFRs (e.g., Manara et al. 2018b; Galli et al. 2020; Luhman & Esplin 2020). We also note that the radially expanding population missed by Spitzer is unlikely

to represent a younger population formed as a consequence of the supernova and/or feedback from the massive OB stars, as Dolan & Mathieu (1999, 2001) found no evidence for triggered or sequential star formation in the region.

We identify interlopers in the Spitzer sample by using distances from Gaia DR2 to find contaminant background sources, a method that was previously applied to refine membership in the Lupus clouds (Manara et al. 2018b). While the individual Gaia DR2 parallaxes of  $\lambda$  Orionis members remain imprecise due to the cluster’s distance, they are sufficient for identifying clear interlopers. We therefore remove five sources (LO 1310, 2357, 2404, 5042, and 7517) from our sample, as the lower bounds of their estimated Gaia DR2 distances from Bailer-Jones et al. (2018)

**Table 1**  
Source Properties

Source	2MASS ID	R.A.	Decl.	SpT	$M_*$ ( $M_\odot$ )	$v_{\text{LSR}}$ ( $\text{km s}^{-1}$ )	Ref. <sup>a</sup>	$\mu_\alpha$ ( $\text{mas yr}^{-1}$ )	$\mu_\delta$ ( $\text{mas yr}^{-1}$ )
LO 65	J05331515+0950301	05:33:15.15	+09:50:30.05	M4	0.19	$11.5 \pm 0.2$	2, 4	$-0.64 \pm 0.28$	$-1.00 \pm 0.23$
LO 1079	J05334791+1001396	05:33:47.91	+10:01:39.69	M5.5	0.07	...	1	$2.11 \pm 0.49$	$-2.68 \pm 0.41$
LO 1152	J05334992+0950367	05:33:49.93	+09:50:36.79	M3.0	0.29	$7.5 \pm 0.1$	1, 4	$2.65 \pm 0.10$	$-3.31 \pm 0.08$
LO 1359	J05335661+1006149	05:33:56.61	+10:06:14.91	M5.25	0.08	...	1	$-0.68 \pm 1.16$	$-1.90 \pm 0.83$
LO 1589	J05340393+0952122	05:34:03.94	+09:52:12.30	M2.5	0.35	$8.2 \pm 0.3$	1, 4	$2.82 \pm 0.12$	$-3.25 \pm 0.09$
LO 1624	J05340495+0957038	05:34:04.96	+09:57:03.76	M3	0.29	$12.0 \pm 0.1$	2, 4	$0.27 \pm 0.07$	$-2.14 \pm 0.06$
LO 1840	J05341141+0942079	05:34:11.41	+09:42:07.94	M6.0	0.09	...	1	$1.24 \pm 0.25$	$-2.91 \pm 0.21$
LO 2088	J05341927+0948275	05:34:19.27	+09:48:27.51	M7.0	0.04	$12.1 \pm 0.5$	1, 5	$-2.06 \pm 1.52$	$-1.03 \pm 1.32$
LO 7957	...	05:34:36.28	+09:55:32.20	M8.0	...	...	1	...	...
LO 2712	J05343836+0958116	05:34:38.36	+09:58:11.63	M7	0.04	...	2	$2.85 \pm 2.18$	$-5.91 \pm 1.85$
LO 2989	J05344621+0955376	05:34:46.21	+09:55:37.65	M5.5	0.07	$12.7 \pm 0.4$	1, 5	$-0.63 \pm 1.01$	$-1.62 \pm 0.85$
LO 2993	J05344631+1002318	05:34:46.32	+10:02:31.87	M5.0	0.08	...	1	$-1.79 \pm 0.69$	$-3.57 \pm 0.60$
LO 3360	J05345639+0955045	05:34:56.40	+09:55:04.46	M4.0	0.19	$10.7 \pm 0.1$	1, 4	$0.84 \pm 0.33$	$-2.65 \pm 0.25$
LO 3506	J05350015+0952408	05:35:00.16	+09:52:40.88	M8	0.03	$13.3 \pm 0.7$	2, 5	$5.26 \pm 3.29$	$0.12 \pm 2.76$
LO 3597	J05350274+0956475	05:35:02.74	+09:56:47.58	M4.0	0.19	$12.3 \pm 0.2$	1, 4	$0.57 \pm 0.12$	$-2.00 \pm 0.10$
LO 3746	J05350707+0954014	05:35:07.07	+09:54:01.48	M6	0.06	$12.7 \pm 0.4$	2, 5	$0.56 \pm 0.62$	$-1.84 \pm 0.49$
LO 7951	...	05:35:07.95	+10:00:06.26	M6.0	...	...	1	...	...
LO 3785	J05350833+0942537	05:35:08.34	+09:42:53.79	K4	1.04	$14.5 \pm 0.3$	2, 4	$1.59 \pm 0.07$	$-1.96 \pm 0.06$
HD 245185	J05350960+1001515	05:35:09.60	+10:01:51.43	A0	2.26	...	3	$0.34 \pm 0.14$	$-1.93 \pm 0.10$
LO 3887	J05351112+0957195	05:35:11.13	+09:57:19.58	M5.0	0.09	$12.8 \pm 0.4$	1, 5	$0.58 \pm 0.37$	$-2.19 \pm 0.33$
LO 3942	J05351255+0953111	05:35:12.56	+09:53:11.14	M3.0	0.30	$11.2 \pm 0.3$	1, 4	$1.44 \pm 0.60$	$-2.96 \pm 0.46$
LO 4021	J05351533+0948369	05:35:15.33	+09:48:36.96	M3.0	0.33	$11.6 \pm 0.3$	1, 5	$0.65 \pm 0.21$	$-1.96 \pm 0.16$
LO 4111	J05351792+0956571	05:35:17.92	+09:56:57.20	M4	0.19	$12.0 \pm 0.3$	2, 5	$1.13 \pm 0.23$	$-1.94 \pm 0.17$
LO 4126	J05351818+0952241	05:35:18.18	+09:52:24.17	M2.0	0.44	$11.7 \pm 0.4$	1, 5	$0.50 \pm 0.21$	$-1.70 \pm 0.16$
LO 4155	J05351904+0954550	05:35:19.05	+09:54:55.74	K2	1.40	$12.9 \pm 0.5$	1, 4	$0.93 \pm 0.08$	$-2.19 \pm 0.06$
LO 4163	J05351913+0954424	05:35:19.14	+09:54:42.38	M4.0	0.19	$11.2 \pm 0.4$	1, 5	$0.21 \pm 0.20$	$-2.03 \pm 0.16$
LO 4187	J05351991+1002364	05:35:19.92	+10:02:36.51	M1.0	0.50	$9.2 \pm 0.3$	1, 6	$2.66 \pm 0.09$	$-2.76 \pm 0.07$
LO 4255	J05352151+0953291	05:35:21.52	+09:53:29.21	M5	0.10	$12.1 \pm 0.3$	2, 5	$0.12 \pm 0.36$	$-1.47 \pm 0.35$
LO 4363	J05352440+0953519	05:35:24.41	+09:53:51.94	M5.5	0.07	$12.3 \pm 0.4$	1, 5	$0.35 \pm 0.64$	$-0.18 \pm 0.50$
LO 4407	J05352536+1008383	05:35:25.36	+10:08:38.25	M3	0.29	$11.2 \pm 0.2$	2, 4	$1.71 \pm 0.54$	$-4.05 \pm 0.43$
LO 4520	J05352846+1002275	05:35:28.46	+10:02:27.44	M3.5	0.25	...	1	$0.62 \pm 0.16$	$-1.56 \pm 0.12$
LO 4531	J05352877+0954101	05:35:28.78	+09:54:10.08	M5.5	0.07	$11.9 \pm 0.3$	1, 5	$1.51 \pm 0.71$	$-2.74 \pm 0.62$
LO 4817	J05353722+0956517	05:35:37.23	+09:56:51.72	M4	0.20	...	2	$0.82 \pm 0.20$	$-2.28 \pm 0.16$
LO 4916	J05353984+0953240	05:35:39.85	+09:53:24.06	M6.5	0.05	$11.8 \pm 0.7$	1, 5	...	...
LO 5267	J05355094+0938567	05:35:50.95	+09:38:56.69	M4	0.19	...	1	$0.87 \pm 0.28$	$-1.77 \pm 0.21$
LO 5447	J05355585+0956217	05:35:55.86	+09:56:21.75	M1.5	0.24	$10.8 \pm 0.2$	1, 4	$0.98 \pm 0.13$	$-1.87 \pm 0.10$
LO 5679	J05360288+0942074	05:36:02.88	+09:42:07.50	M1	0.47	$11.4 \pm 0.1$	2, 4	$2.16 \pm 0.09$	$-2.28 \pm 0.06$
LO 5916	J05360981+0942370	05:36:09.81	+09:42:37.02	M6.0	0.05	$11.8 \pm 0.5$	1, 5	$0.58 \pm 1.07$	$-2.09 \pm 0.98$
LO 6191	J05361810+0952254	05:36:18.11	+09:52:25.41	M6.0	0.06	$11.9 \pm 0.5$	1, 5	$1.39 \pm 0.82$	$-3.26 \pm 0.61$
LO 6866	J05363804+0940509	05:36:38.07	+09:40:50.18	K7	0.67	$11.9 \pm 0.2$	2, 4	$0.60 \pm 0.12$	$-1.79 \pm 0.11$
LO 6886	J05363861+0935052	05:36:38.61	+09:35:05.22	M3	0.29	$11.5 \pm 0.2$	2, 4	$0.83 \pm 0.44$	$-2.14 \pm 0.36$
LO 7402	J05365309+0941556	05:36:53.09	+09:41:55.67	K4	1.05	$13.6 \pm 0.1$	2, 4	$1.96 \pm 0.06$	$-1.97 \pm 0.05$
LO 7490	J05365533+0946479	05:36:55.34	+09:46:47.94	M3	0.33	...	1	$1.15 \pm 0.18$	$-2.54 \pm 0.17$
LO 7528	J05365617+0931227	05:36:56.17	+09:31:22.70	M1.5	0.42	$9.5 \pm 0.2$	1, 4	...	...

**Note.**

<sup>a</sup> References for stellar SpTs and radial velocities ( $v_{\text{LSR}}$ ): (1) Bayo et al. (2011), (2) Hernández et al. (2010), (3) Hernández et al. (2009), (4) Kounkel et al. (2018), (5) Maxted et al. (2008), (6) Sacco et al. (2008).

are  $>480$  pc, making them likely background sources. Indeed, LO 1310 and 2357 have radial velocities in the local standard of rest (LSR) reference frame of  $v_{\text{LSR}} = 1.3$  and  $-35$   $\text{km s}^{-1}$ , respectively, which differ significantly from the average cluster value of  $12$   $\text{km s}^{-1}$  (Kounkel et al. 2018); LO 2404, 5042, and 7517 do not have known radial velocities. We also remove LO 3710, found to be a nonmember by Bayo et al. (2011) due to a discrepant surface gravity. Of these interlopers, only LO 7517 is detected by our ALMA survey at marginal ( $3.4\sigma$ ) significance; given its estimated Gaia DR2 distance of  $3744_{-336}^{+405}$  pc, it is likely a background galaxy.

Table 1 gives our final sample of the 44 protoplanetary disks analyzed in the remainder of this work.

**3.2. Host Star Properties**

The available host star properties for our disk sample are provided in Table 1. Stellar spectral types (SpTs) were mostly determined by Bayo et al. (2011) from moderate-resolution optical and near-infrared spectra. However, 14 stars have only photometric SpTs from Hernández et al. (2010), who interpolated  $R - J$  colors onto the SpT sequence using the standard  $R - J$  colors from Kenyon & Hartmann (1995). Although the  $R - J$  colors were not corrected for reddening, the reddening toward  $\lambda$  Orionis is low at  $E(B - V) \approx 0.12$  (DiPlas & Savage 1994), and these photometric SpTs match well (typically  $\pm 1$  spectral subtype) to the spectroscopically determined values from Bayo et al. (2011) when the samples overlap.

The host star proper motions in R.A. ( $\mu_\alpha$ ) and decl. ( $\mu_\delta$ ) are from Gaia DR2. Radial velocities are also provided and taken from various literature sources, translated into the LSR reference frame ( $v_{\text{LSR}}$ ) using the source coordinates. The source coordinates in R.A. and decl. are the fitted positions for our ALMA detections (Section 4.2) or the Two Micron All Sky Survey (2MASS) positions for the nondetections.

As previously mentioned, the  $\lambda$  Orionis cluster is too distant for reliable individual Gaia DR2 parallaxes. This is further complicated for young disk-hosting stars whose variability from disk scattered light and/or surrounding nebulosity can result in poor fits to the Gaia DR2 single-star astrometric model, leading to higher astrometric noise. Thus, we do not provide distance estimates for each source in our sample but instead rely on the average distance of the non-disk-bearing members in  $\lambda$  Orionis from Gaia DR2, which is well constrained to  $404 \pm 4$  pc (Kounkel et al. 2018) and consistent with earlier estimates of  $450 \pm 50$  pc based on main-sequence fitting to the massive OB stars (Dolan & Mathieu 2001; Mathieu 2015). We therefore adopt a distance of 400 pc for  $\lambda$  Orionis in the remainder of this work.

We estimate stellar masses ( $M_\star$ ) from these SpT values and 2MASS (Skrutskie et al. 2006)  $J$ -band magnitudes, following the methods of Ansdell et al. (2017). Each target is placed on the Hertzsprung–Russell (H-R) diagram by converting SpT to stellar effective temperature and  $J$ -band magnitude to stellar luminosity using the relations from Herczeg & Hillenbrand (2015) and a distance of 400 pc. Estimates of  $M_\star$  are then found by comparing the positions on the H-R diagram to the evolutionary models of Baraffe et al. (2015). For the one intermediate-mass star in our sample, HD 245185, we instead use the evolutionary models of Siess et al. (2000). We do not provide  $M_\star$  estimates for the two sources in our sample without 2MASS data (LO 7957 and 7951). The typical  $M_\star$  uncertainties, propagated from the uncertainties on SpT and  $J$ -band magnitude, are 0.1–0.2  $M_\odot$ .

## 4. ALMA Observations and Results

### 4.1. ALMA Observations

The ALMA observations used in this work were taken during Cycle 5 under program 2017.1.00466.S (PI: Ansdell). The program allowed for a range of array configurations to maximize the probability of survey completion, and the observations were conducted over 13 execution blocks (see Appendix A for information on the array configuration and weather conditions for each execution block). All sources in our sample were observed during each execution block, such that the sensitivities and synthesized beams are uniform across the sample.

The spectral setup was identical for each execution block; four spectral windows were centered on 247.96, 245.46, 232.97, and 230.51 GHz, each with usable bandwidths of 1.88 GHz, for a bandwidth-weighted mean continuum frequency of 239.36 GHz (1.25 mm). The last spectral window covered the  $^{12}\text{CO } J = 2 - 1$  transition at moderate ( $\sim 1$  km s $^{-1}$ ) spectral resolution to preserve the maximum possible continuum bandwidth while allowing for the possibility of detecting molecular gas emission.

On-source integration times were  $\sim 6$  per source, chosen so the  $3\sigma$  dust mass constraints would be comparable to the limits reached in the ALMA surveys of more nearby SFRs (e.g., Ansdell et al. 2016; Barenfeld et al. 2016; Pascucci et al. 2016), assuming a linear relation between millimeter flux and dust mass (e.g., Hildebrand 1983). Data were pipeline-calibrated by NRAO staff using the Common Astronomy Software Applications (CASA)

**Table 2**  
ALMA Disk Fluxes

Source	$F_{1.25 \text{ mm}}$ (mJy)	$F_{^{12}\text{CO}}$ (mJy km s $^{-1}$ )
LO 65	0.117 $\pm$ 0.030	<25
LO 1079	0.033 $\pm$ 0.030	<24
LO 1152	0.159 $\pm$ 0.028	<24
LO 1359	0.053 $\pm$ 0.028	<23
LO 1589	0.053 $\pm$ 0.028	<24
LO 1624	1.179 $\pm$ 0.028	<24
LO 1840	−0.008 $\pm$ 0.030	<24
LO 2088	−0.005 $\pm$ 0.028	<24
LO 7957	0.075 $\pm$ 0.028	<24
LO 2712	−0.033 $\pm$ 0.028	<25
LO 2989	0.076 $\pm$ 0.028	<23
LO 2993	0.008 $\pm$ 0.030	<24
LO 3360	0.234 $\pm$ 0.028	<24
LO 3506	0.016 $\pm$ 0.030	<25
LO 3597	−0.063 $\pm$ 0.030	<25
LO 3746	0.047 $\pm$ 0.030	<24
LO 7951	0.038 $\pm$ 0.028	<25
LO 3785	0.035 $\pm$ 0.034	<28
HD 245185	33.955 $\pm$ 0.056	1915 $\pm$ 51
LO 3887	0.024 $\pm$ 0.028	<23
LO 3942	−0.001 $\pm$ 0.028	<24
LO 4021	0.032 $\pm$ 0.028	<24
LO 4111	−0.012 $\pm$ 0.028	<24
LO 4126	0.004 $\pm$ 0.028	<23
LO 4155	0.927 $\pm$ 0.030	27 $\pm$ 8
LO 4163	0.481 $\pm$ 0.028	<24
LO 4187	1.846 $\pm$ 0.037	113 $\pm$ 21
LO 4255	0.099 $\pm$ 0.028	<24
LO 4363	0.032 $\pm$ 0.028	<23
LO 4407	1.067 $\pm$ 0.037	29 $\pm$ 8
LO 4520	0.340 $\pm$ 0.028	<25
LO 4531	0.375 $\pm$ 0.028	<22
LO 4817	0.023 $\pm$ 0.028	<24
LO 4916	0.017 $\pm$ 0.028	<24
LO 5267	0.257 $\pm$ 0.028	<24
LO 5447	−0.002 $\pm$ 0.028	<23
LO 5679	0.054 $\pm$ 0.028	<24
LO 5916	0.011 $\pm$ 0.028	<23
LO 6191	0.009 $\pm$ 0.028	<24
LO 6866	0.623 $\pm$ 0.028	80 $\pm$ 14
LO 6886	0.006 $\pm$ 0.028	<23
LO 7402	0.017 $\pm$ 0.030	<23
LO 7490	0.030 $\pm$ 0.028	<25
LO 7528	0.031 $\pm$ 0.028	<25

package (McMullin et al. 2007) version 5.4.0. The pipeline included flux, bandpass, and gain calibrations (see Appendix A for a list of the calibrators). We assume an absolute flux calibration uncertainty of 10%, similar to other ALMA disk surveys (e.g., Ansdell et al. 2016; Barenfeld et al. 2016; Cazzoletti et al. 2019).

### 4.2. ALMA Continuum Results

We create continuum images from the calibrated visibilities by averaging over the continuum channels using the `split` task in CASA, then cleaning with a Briggs robust weighting parameter of +0.5 using the `tclean` task. This results in a median continuum rms of 34  $\mu$ Jy and beam size of  $0.''31 \times 0.''29$ . We do not perform self-calibration, as the detected sources are faint, with a median signal-to-noise ratio of 15 (see Table 2).

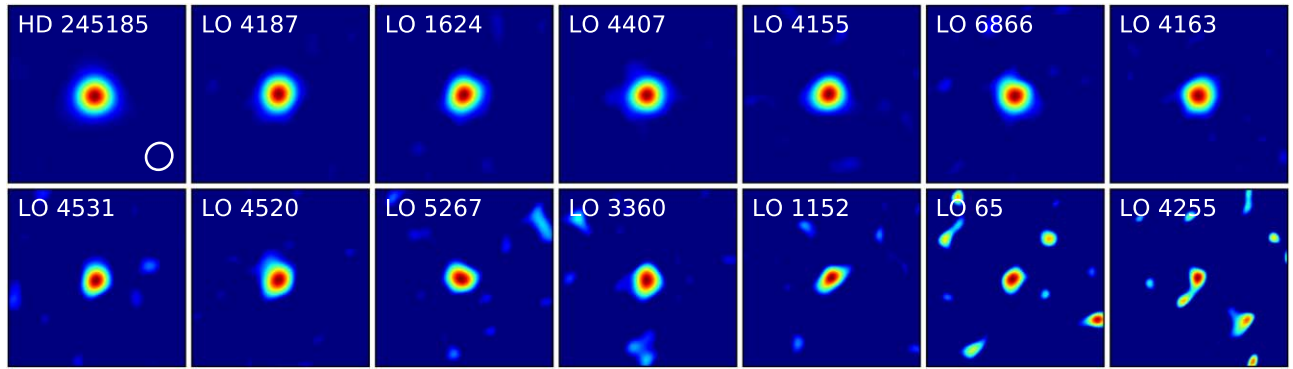


**Figure 2.** ALMA 1.25 mm continuum images of the 14 detected disks in our  $\lambda$  Orionis sample, ordered by decreasing flux density (as reported in Table 2). The  $2'' \times 2''$  images are centered on the source, scaled to their maximum value, and clipped below  $1.5\sigma$  for clarity. The typical beam size of  $\sim 0.3''$  is shown in the first panel by the white ellipse.

In most cases, we measure continuum flux densities by fitting point-source models to the visibility data with the `uvmodelfit` task in CASA. The point-source model has three free parameters: integrated flux density ( $F_{1.25\text{ mm}}$ ), R.A. offset from the phase center ( $\Delta\alpha$ ), and decl. offset from the phase center ( $\Delta\delta$ ). For the nondetections, we fix  $\Delta\alpha$  and  $\Delta\delta$  to zero when running `uvmodelfit` to avoid spurious detections (the phase offsets are typically only  $0.05''$  for the detections, much smaller than the beam size). In three cases, the sources are resolved; therefore, we use an elliptical Gaussian model instead, which has three additional parameters: FWHM along the major axis ( $a$ ), aspect ratio of the axes ( $r$ ), and position angle (P.A.). With the underlying assumption that these models describe the data appropriately, we multiply the uncertainties on all of the fitted parameters by the factor needed to produce a reduced  $\chi^2$  of 1 (typically a factor of 2).

Table 2 reports the  $F_{1.25\text{ mm}}$  values for all sources, along with their statistical uncertainties (i.e., not including the 10% flux calibration error), while Figure 2 shows the continuum images for the  $\geq 3\sigma$  detections. Only 14 of the 44 sources are detected at  $\geq 3\sigma$  significance, and only three of the detections are marginally resolved. We conservatively identify resolved sources as those where the ratio of  $a$  to its uncertainty is greater than 5. The resolved sources are HD 245185, LO 4187, and LO 4407, with the following fitted elliptical Gaussian parameters, respectively:  $a = 0.203 \pm 0.002$ ,  $0.113 \pm 0.015$ , and  $0.123 \pm 0.022$ ;  $r = 0.807 \pm 0.006$ ,  $0.710 \pm 0.196$ , and  $0.508 \pm 0.380$ ; and P.A. =  $70.1 \pm 0.9$ ,  $-1.3 \pm 19.5$ , and  $85.5 \pm 18.7$ .

We stack the images of the 30 nondetections to constrain the average continuum flux for the individually undetected sources, finding a tentative detection of  $0.019 \pm 0.006$  mJy ( $3.2\sigma$ ) in the stacked image. We verify this result by calculating the mean continuum flux density and standard error on the mean for the 30 nondetections using the values in Table 2, which gives  $0.020 \pm 0.005$  mJy ( $4.0\sigma$ ).

#### 4.3. ALMA CO Results

We extract  $^{12}\text{CO}$  channel maps from the calibrated visibilities by first subtracting the continuum using the `uvcontsub` task in CASA. To search for  $^{12}\text{CO}$  emission, we follow the general procedure of Ansdell et al. (2017). In short, we extract an initial spectrum for each source to identify candidate detections with emission exceeding  $3\times$  the channel rms near the expected  $v_{\text{LSR}}$  of the cluster ( $12\text{ km s}^{-1}$ ; Kounkel et al. 2018). These candidates are visually inspected, and any emission is cleaned with a Briggs robust weighting parameter of +0.5 using `tclean`. Zero-moment

maps are then created by summing the channels  $\pm 3\text{ km s}^{-1}$  from the systemic velocity unless clear emission was seen beyond these limits. The integrated  $^{12}\text{CO}$  line fluxes ( $F_{^{12}\text{CO}}$ ) are measured using a curve-of-growth aperture photometry method, with errors ( $E_{^{12}\text{CO}}$ ) estimated by taking the standard deviation of fluxes measured within the same-sized aperture placed randomly within the field of view but away from the source.

Only five sources (HD 245185, LO 4155, LO 4187, LO 4407, and LO 6866) are detected with  $F_{^{12}\text{CO}} \geq 3 \times E_{^{12}\text{CO}}$ , though two of these (LO 4155 and 4407) are marginal ( $3\sigma$ – $4\sigma$ ) detections. One other source, LO 1624, shows emission at  $\sim 5\times$  the rms in the single channel at its known  $v_{\text{LSR}}$  but is undetected in its zero-moment map, as summing over several channels dilutes the emission. For the nondetections, we construct zero-moment maps by integrating  $\pm 3\text{ km s}^{-1}$  from their known  $v_{\text{LSR}}$  when available (see Table 1), otherwise from the average  $v_{\text{LSR}}$  of the cluster ( $12\text{ km s}^{-1}$ ; Kounkel et al. 2018). Table 2 gives the  $F_{^{12}\text{CO}}$  measurements for the detections and upper limits of  $3\times$  the rms in the zero-moment maps for the nondetections. Figure 3 shows the zero- and first-moment maps for the five detections, while Appendix B presents the  $^{12}\text{CO}$  spectra for all sources in our sample.

Figure 4 then shows ALMA Band 6  $^{12}\text{CO}$  emission as a function of the Band 6 continuum for the continuum-detected disks in the evolved  $\lambda$  Orionis cluster (this work), the young Lupus clouds (Ansdell et al. 2018), and the middle-aged  $\sigma$  Orionis cluster (Ansdell et al. 2017; M. Ansdell et al., 2020 in preparation), all scaled to 150 pc. We do not show other notable ALMA disk surveys, as they were conducted in Band 7 (e.g., Barenfeld et al. 2016; Pascucci et al. 2016) or do not have published Band 6  $^{12}\text{CO}$  fluxes (e.g., Cieza et al. 2019). Interestingly, the roughly linear correlation between continuum and  $^{12}\text{CO}$  emission holds over the first  $\sim 5$  Myr of disk evolution, implying that the lack of gas detections in our  $\lambda$  Orionis survey can be explained by the low continuum emission.

This roughly linear correlation between the (somewhat) optically thin millimeter continuum flux and the optically thick  $^{12}\text{CO}$  flux is potentially due to more massive dust disks having more extended gas disks (e.g., Barenfeld et al. 2016). Moreover, since there is an observed linear relationship between the millimeter continuum luminosity ( $L_{\text{mm}}$ ) and emitting surface area ( $R_{\text{mm}}^2$ ) of protoplanetary disks (Tripathi et al. 2017; Andrews et al. 2018a), and Figure 4 implies that the  $^{12}\text{CO}$  luminosity ( $L_{\text{CO}}$ ) is proportional to  $L_{\text{mm}}$ , while we also expect  $L_{\text{CO}}$  to be proportional to the  $^{12}\text{CO}$  emitting surface area ( $R_{\text{CO}}^2$ ) if it is optically thick, we can predict that  $R_{\text{CO}} \propto R_{\text{mm}}$ ,

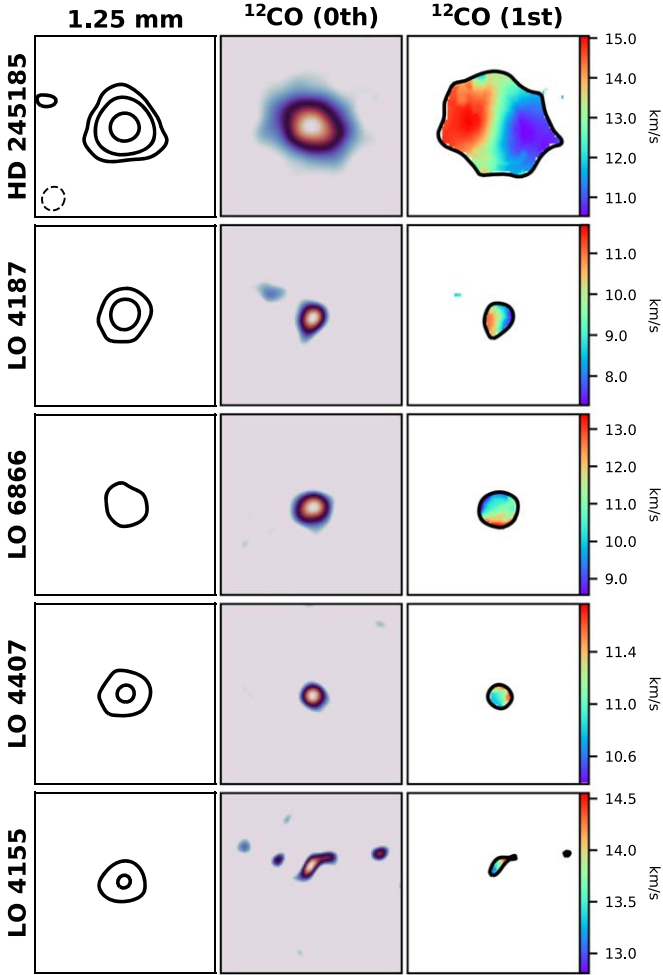


**Figure 3.** Our ALMA Band 6 observations of the five  $^{12}\text{CO}$  detections in our sample (Section 4.3). The first column shows the 1.25 mm continuum maps with  $4\sigma$ ,  $20\sigma$ , and  $150\sigma$  contours. The middle column shows the  $^{12}\text{CO}$  zero-moment maps, scaled to their maximum value and clipped below  $2\sigma$  for clarity. The final column shows the  $^{12}\text{CO}$  first-moment maps within the  $3\sigma$  contours of the zero-moment maps. Images are  $2'' \times 2''$ , and the typical beam size is given in the first panel by the dashed ellipse.

which is indeed seen in observations (Ansdell et al. 2018; Trapman et al. 2020).

## 5. Disk Properties

### 5.1. Dust Masses

Under the simplified assumption that dust emission from a protoplanetary disk at millimeter wavelengths is optically thin and isothermal, the observed continuum flux density at a given frequency ( $F_\nu$ ) can be directly related to the mass of the emitting dust ( $M_{\text{dust}}$ ), as established in Hildebrand (1983),

$$M_{\text{dust}} = \frac{F_\nu d^2}{\kappa_\nu B_\nu(T_{\text{dust}})} \approx 4.1 \times F_{1.25\text{mm}}, \quad (1)$$

where  $M_{\text{dust}}$  is in Earth masses and  $F_{1.25\text{mm}}$  is in mJy. Here we use  $B_\nu(T_{\text{dust}})$  as the Planck function for a characteristic dust temperature of  $T_{\text{dust}} = 20$  K, the median for Taurus disks (Andrews & Williams 2005). We take the dust grain opacity,  $\kappa_\nu$ , as  $2.3\text{ cm}^2\text{ g}^{-1}$  at 230 GHz and use an opacity power-law index of  $\beta_d = 1.0$  (Beckwith et al. 1990); these are the same assumptions as

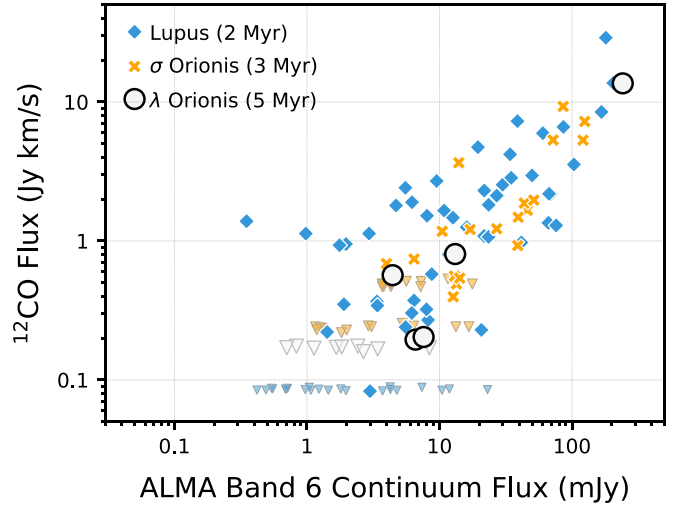


**Figure 4.** The  $^{12}\text{CO}$  flux as a function of continuum flux in ALMA Band 6 for the continuum-detected disks in Lupus (Ansdell et al. 2018),  $\sigma$  Orionis (Ansdell et al. 2017; M. Ansdell et al., 2020 in preparation), and  $\lambda$  Orionis (this work). Fluxes are normalized to 150 pc, and downward-facing triangles are  $3\sigma$  upper limits on the  $^{12}\text{CO}$  flux. Approximate ages of each region are provided for reference. The four  $\lambda$  Orionis  $^{12}\text{CO}$  detections follow the roughly linear correlation seen in younger regions, and the lingering bright disk in  $\lambda$  Orionis is HD 245185.

in Ansdell et al. (2016, 2017, 2018) and Cieza et al. (2019) but differ slightly from some previous ALMA disk surveys (Barenfeld et al. 2016; Pascucci et al. 2016), which use  $\beta = 0.4$ . For the distance,  $d$ , we use the cluster’s average Gaia DR2 value of 400 pc (Section 3.2) and take the  $F_{1.25\text{mm}}$  measurements from Table 2.

With this approach, the median  $M_{\text{dust}}$  of the continuum detections in our  $\lambda$  Orionis survey is only  $\sim 2 M_\oplus$ . These dust masses may be underestimated, however, if the observed millimeter continuum emission is (partially) optically thick (e.g., Andrews & Williams 2005; Zhu et al. 2019) and/or the temperature of the dust in the outer disk (where we assume most of the disk mass is located) is lower than 20 K. Nevertheless, employing this simplified relation with these caveats in mind provides the most practical approach given the faint and unresolved emission from the disks in our observations.

Figure 5 shows the  $M_{\text{dust}}$  estimates for the continuum detections in our survey in increasing order. It also includes the median  $3\sigma$  upper limit of  $\sim 0.4 M_\oplus$  for the individual nondetections in our survey, as well as the mean detection of  $\sim 0.08 M_\oplus$  found when stacking these nondetections (Section 4.2).

### 5.2. Comparisons to Other Regions

At  $\sim 5$  Myr old,  $\lambda$  Orionis provides an important point of comparison to the several younger disk populations, as well as the similarly aged Upper Sco disk population, that have been previously surveyed by ALMA. Figure 6 compares the  $M_{\text{dust}}$  cumulative distribution for  $\lambda$  Orionis (this work) to that of OMC-2 (van Terwisga et al. 2019a), Lupus (Ansdell et al. 2018),  $\sigma$  Orionis (Ansdell et al. 2017), and Upper Sco (Barenfeld et al. 2016). The  $M_{\text{dust}}$  values are uniformly calculated using Equation (1) with the reported wavelengths of the surveys and typical Gaia DR2 distances of  $\sim 150$  pc for Lupus and Upper Sco and  $\sim 400$  pc for  $\sigma$  Orionis and OMC-2. For the approximate ages of the regions, we adopt the values used in the ALMA surveys or reported in more recent analyses of the protoplanetary disk populations (e.g.,

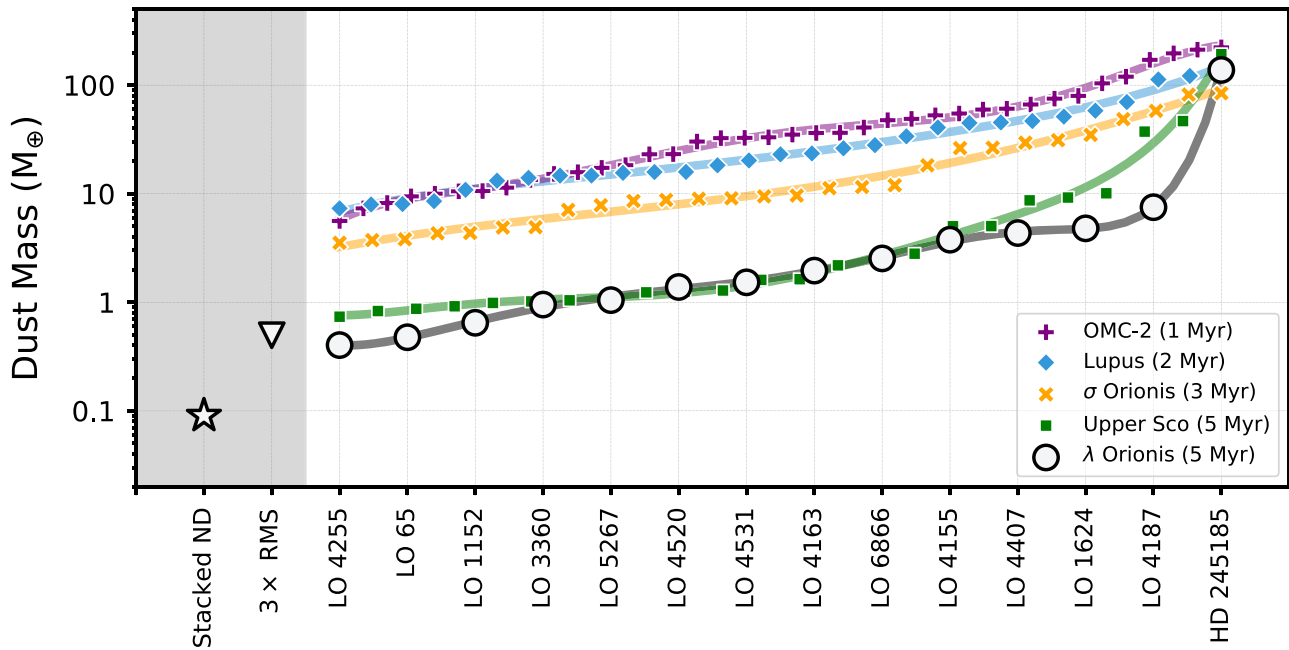


**Figure 5.** Dust masses of the 14 continuum-detected disks in our  $\lambda$  Orionis survey (white circles) in increasing order (source names are given on the  $x$ -axis). The white downward-facing triangle is the median  $3\sigma$  upper limit for individual nondetections, while the white star shows their detected average dust mass from our stacking analysis (Section 5.1). Comparable disk dust mass populations (see Section 5.2) from OMC-2 (purple plus signs), Lupus (blue diamonds),  $\sigma$  Orionis (orange crosses), and Upper Sco (green squares) are also shown, illustrating the smooth distribution in the younger regions in contrast with the steep rise toward the high-mass outlier disks in the older populations (see Sections 5.2 and 6.3). The colored solid lines are polynomial fits to guide the eye for each region; the approximate ages of each region are also provided for reference.

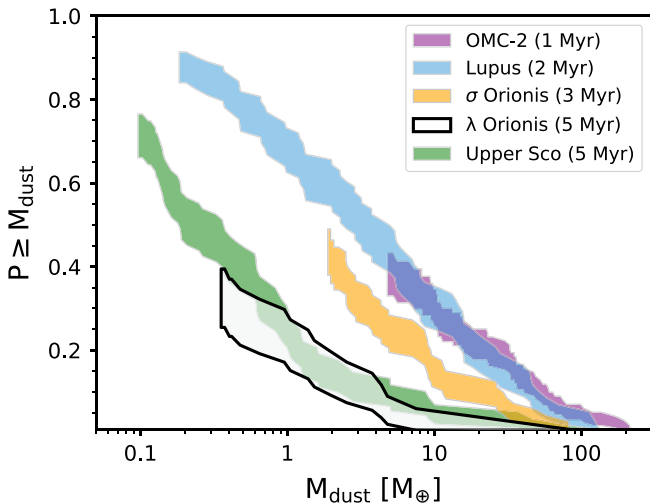


**Figure 6.** Disk dust mass ( $M_{\text{dust}}$ ) cumulative distribution for  $\lambda$  Orionis compared to several other regions surveyed by ALMA, calculated with the Kaplan–Meier Estimator to account for upper limits (see Section 5.2). Approximate ages for each region are provided for reference.

Andrews 2020). The cumulative distributions are constructed using the Kaplan–Meier Estimator (with the Python `lifelines` package; Davidson-Pilon et al. 2020) to account for upper limits, as in previous works (e.g., Barenfeld et al. 2016; Ansdell et al. 2017; Cazzoletti et al. 2019; Cieza et al. 2019; van Terwisga et al. 2019b).

Figure 6 illustrates that  $\lambda$  Orionis follows the general decay in the overall disk dust mass population with age that has been previously reported (e.g., Ansdell et al. 2016; Barenfeld et al. 2016; Pascucci et al. 2016; Cieza et al. 2019; van Terwisga et al. 2019b). Moreover, the  $M_{\text{dust}}$  distribution in  $\lambda$  Orionis is statistically indistinguishable from that of the similarly aged

Upper Sco association. Both of these findings suggest that, if a supernova did occur relatively recently in  $\lambda$  Orionis, it did not have a significant impact on disk dust mass evolution in the region. We discuss this further in Section 6.1.

A reliable comparison of the  $M_{\text{dust}}$  distributions in Figure 6 requires confirming that the regions have similar  $M_*$  populations, due to the known correlation between disk dust mass and stellar mass (e.g., Andrews et al. 2013; Ansdell et al. 2016; Barenfeld et al. 2016; Pascucci et al. 2016). Two-sample tests have previously demonstrated that the stellar mass populations in Lupus,  $\sigma$  Orionis, and Upper Sco are likely drawn from the same parent population (Ansdell et al. 2016, 2017; Barenfeld et al. 2016). To confirm that the  $M_{\text{dust}}$  populations in  $\lambda$  Orionis and Upper Sco are indeed statistically indistinguishable, we again use two-sample tests to compare their stellar mass populations. Using the  $M_*$  values from Table 1 for  $\lambda$  Orionis and those from Barenfeld et al. (2016) for Upper Sco, we find  $p$ -values of 0.77 and 0.11 for the T-test and Wilcoxon rank-sum test, respectively (calculated with `scipy.stats` in Python). Thus, the  $M_*$  populations are likely drawn from the same parent population, so the  $M_{\text{dust}}$  distributions can be reliably compared.

Figure 5 also illustrates the decline in  $M_{\text{dust}}$  distributions with age, but it highlights differences at the high-mass end that are not readily apparent from the cumulative distributions in Figure 6. In Figure 5, the  $\lambda$  Orionis detections are plotted against the upper 32% of the  $M_{\text{dust}}$  populations in the comparison regions (32% was chosen to match the detection rate in  $\lambda$  Orionis). Interestingly, the highest-mass disks in all of the regions appear to converge around  $\sim 100 M_{\oplus}$  regardless of age or environment. Although the number of disks at such high masses falls steeply after a few Myr, one or more “outlier” disks appear to persist even at  $\sim 5$  Myr of age. We discuss these lingering massive disks in Section 6.3.

One caveat to keep in mind is that the ages assumed in this work are just the typical median values of the regions reported in the literature. They do not reflect the possibility of distributed age populations and have been calculated using different methods, any of which are likely imprecise and/or inaccurate due to biases in both the observations and the stellar evolution models (e.g., Bell et al. 2013). However, the relative ages should be generally reliable and sufficient for the purposes of this work.

### 5.3. HD 245185

The star HD 245185 hosts a clear outlier disk in  $\lambda$  Orionis, having over an order of magnitude higher millimeter continuum and  $^{12}\text{CO}$  flux than the rest of the sample (Figure 4). It is a well-studied Herbig Ae/Be star in the literature and the only early-type (A0) star in our sample (Table 1) with a mass of  $\sim 2.5 M_{\odot}$  (e.g., Folsom et al. 2012). Figure 3 shows the 1.25 mm continuum map and the  $^{12}\text{CO}$  zero- and first-moment maps from our ALMA observations. We note that the proper motions ( $\mu_{\alpha} = 0.34$ ,  $\mu_{\delta} = -1.93$ ) and distance ( $427^{+21}_{-19}$  pc) from Gaia DR2, as well as the systemic velocity derived from our ALMA  $^{12}\text{CO}$  observations ( $v_{\text{LSR}} \approx 13 \text{ km s}^{-1}$ ), are all consistent with cluster membership.

Equation (1) yields  $M_{\text{dust}} \approx 140 M_{\oplus}$ , an order of magnitude higher than the next most massive disk in  $\lambda$  Orionis (Figure 5). One concern is that this is due to HD 245185 being the only hot star in our sample, given that the simplified relation in Equation (1) assumes  $T_{\text{dust}} = 20 \text{ K}$  for all disks. However, only some of the difference (a factor of  $\sim 3$ ) may be accounted for if, rather than assuming an isothermal disk, we scale the dust temperature with stellar luminosity using  $T_{\text{dust}} = 25 \text{ K} \times (L_{\star}/L_{\odot})^{0.25}$  as suggested by the radiative transfer model grid of Andrews et al. (2013). We do not use this scaling, however, as it remains uncertain whether such a clear relationship holds in the real disk population. For example, Tazzari et al. (2017) found no relation between  $T_{\text{dust}}$  and stellar properties when modeling the ALMA visibilities of resolved Lupus disks.

Another reason why a massive disk around HD 245185 at the evolved age of  $\lambda$  Orionis is unusual is that disks around intermediate-mass stars typically dissipate twice as fast as those around late-type stars (at least based on infrared emission, which traces the warm inner disk; e.g., Ribas et al. 2015). It is unlikely that HD 245185 is simply much younger than the average disk in the cluster; several authors have estimated the age of HD 245185, for example,  $6.9 \pm 2.5$  (Alecian et al. 2013) and  $5.5 \pm 2.0$  (Folsom et al. 2012) Myr, suggesting that we cannot use delayed star formation relative to the rest of  $\lambda$  Orionis to reconcile this system. We discuss possible explanations for such long-lived primordial disks in Section 6.3.

## 6. Discussion

### 6.1. Do Supernovae Impact Planet Formation?

The cluster  $\lambda$  Orionis may provide a rare snapshot of an evolved SFR that is  $\sim 1$  Myr post-supernova with the remaining OB stars, lower-mass stellar population, and remnant molecular cloud all still present (Section 2). Comparing the disk population in  $\lambda$  Orionis to those in other SFRs may therefore provide an opportunity to study how supernovae affect planet formation.

Supernovae are theorized to strip significant amounts of mass from disks around nearby pre-main-sequence stars.

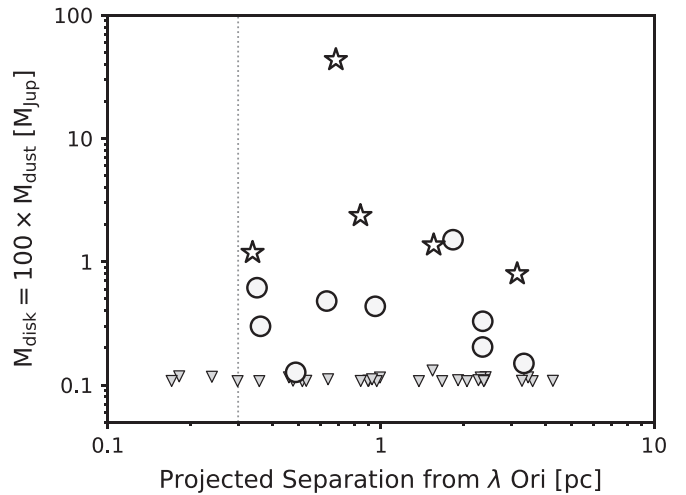


**Figure 7.** Disk mass ( $M_{\text{disk}}$ ), assuming a gas-to-dust ratio of 100, as a function of projected separation from the central OB star ( $\lambda$  Ori) in  $\lambda$  Orionis. Circles are ALMA Band 6 continuum detections, and downward-facing triangles are  $3\sigma$  upper limits; stars indicate  $^{12}\text{CO}$  detections. The vertical dotted line denotes the 0.3 pc distance of the supernova in the simulations of Close & Pittard (2017; see Section 6.1).

Close & Pittard (2017) ran three-dimensional hydrodynamic simulations of protoplanetary disks, with a range of masses and inclinations, subject to a supernova occurring 0.3 pc away. They reported an “instantaneous stripping” phase with mass-loss rates of  $10^{-5} M_{\odot} \text{ yr}^{-1}$  lasting 10–100 yr, followed by more moderate but extended ablation with mass-loss rates of  $10^{-6}$ – $10^{-7} M_{\odot} \text{ yr}^{-1}$ . For the low-mass ( $0.1 M_{\text{Jup}}$ ) and moderate-mass ( $1.0 M_{\text{Jup}}$ ) disks in their simulations, up to 90% and 30% of the disk mass, respectively, was removed during the instantaneous stripping phase; these disk masses are typical in  $\sigma$  Orionis, a possible example of a presupernova OB cluster. High-mass ( $10 M_{\text{Jup}}$ ) disks, however—similar to the outlier around HD 245185 in  $\lambda$  Orionis (Section 5.3)—were largely unaffected. Since the peak ram pressure in the simulations of Close & Pittard (2017) strongly depends on distance from the supernova (dropping off as  $d^{-3}$ ), we would expect most disks within 0.3 pc to be significantly depleted in mass, with those further out relatively unaffected.

Indeed, as shown in Figure 7, we observe but do not detect four disks with projected separations  $< 0.3$  pc from the cluster core, the presumed supernova location (Section 2). Several disks are detected just beyond 0.3 pc but have disk masses similar to the rest of the population. Due to the natural course of cluster expansion, these projected distances are likely overestimates of the source locations when the supernova occurred. Still, our finding that the overall disk population in  $\lambda$  Orionis appears to follow the general decline in disk dust mass with age seen in other SFRs and is statistically indistinguishable from that of the similarly aged Upper Sco association (Figure 6; Section 5.2) implies that a supernova occurring several Myr into disk evolution does not significantly reduce the amount of planet-forming solid material that would otherwise be available at this age, except potentially for disks that were within a small fraction of a parsec from the supernova event.

Additionally, presupernova feedback may mute the effects of the actual supernova event on the surrounding environment. Recent simulations that combine stellar winds and photoionization with supernova events (Lucas et al. 2020) found that

presupernova feedback sculpts low-density channels in the gas through which supernova energy can more freely escape into the wider interstellar medium. As a result, supernova explosions may have only moderate, though more widespread, effects on the surrounding natal molecular clouds and their star/disk populations. When occurring late in disk evolution, it is possible that these moderate effects from supernovae are simply negligible when compared to other disk evolutionary processes.

One caveat to this interpretation, however, is that we cannot rule out that a supernova also occurred in the SFRs against which we are comparing the  $\lambda$  Orionis disk population. In particular, a supernova may have also occurred  $\sim 1$  Myr ago in Upper Sco; this is based on the kinematics of an expanding H I shell in the region (de Geus 1992), as well as the kinematic trace-back of the runaway O-type star  $\zeta$  Oph and pulsar PSR 1932+11059, which may have once been close binaries in Upper Sco before the pulsar progenitor exploded as a supernova (Hoogerwerf et al. 2000, 2001). However, the large uncertainties on the present-day kinematics of the runaway objects, including an unknown radial velocity for the pulsar, make the location of the presumed supernova, and thus its potential impact on the Upper Sco disk population, unclear.

Another caveat is that our ALMA sample is selected from targeted Spitzer observations (Section 3) and thus only includes disks that are currently within  $\sim 3$  pc of the cluster core (see white dashed box in Figure 1). Because the recently identified  $\lambda$  Orionis members outside the Spitzer survey region are radially expanding outward (Figure 1; Kounkel et al. 2018), the concern is that our ALMA survey missed some disks that were once much closer to the cluster core and thus potentially most affected by the supernova. However, the faster-moving stars in this radially expanding population only have typical proper motions of  $\sim 1$  mas yr $^{-1}$  (relative to the cluster median), which translates to  $\sim 2$  pc over 1 Myr at 400 pc. Because these stars also have typical projected separations of  $\gtrsim 10$  pc from the cluster core, it is unlikely that they were particularly close to the supernova when it occurred, especially if the outward acceleration was aided by gravitational feedback of the dispersed gas (Zamora-Avilés et al. 2019). Moreover, although Kounkel et al. (2018) explained the observed radial motions as due to the “single-trigger expansion” caused by the supernova, alternative explanations staged presupernova are also viable; such kinematics can be a consequence of any mechanism that disperses the intracluster gas (e.g., stellar winds or radiation; see Winter et al. 2019), and presupernova feedback may preclude the actual supernova event as the main mechanism driving the removal of the gas potential (e.g., Lucas et al. 2020).

Indeed, an alternative explanation is that a supernova has not yet actually occurred in  $\lambda$  Orionis, and that the observed features described in Section 2 originate from other aspects of the cluster history, such as presupernova feedback. In fact, the expected chemical effects of a supernova are not readily apparent in our current ALMA data. Supernovae are production sites of cosmic rays (see review in Grenier et al. 2015); thus, the cosmic-ray ionization rate of H<sub>2</sub> ( $\zeta_{\text{CR}}$ ) should be enhanced in  $\lambda$  Orionis. Typical ionization rates in molecular clouds are  $\zeta_{\text{CR}} \sim 10^{-17}$  s $^{-1}$  and may be even lower in disk midplanes (Cleeves et al. 2014); however, after a supernova, the levels can be enhanced to  $\zeta_{\text{CR}} \sim 10^{-15}$  or  $10^{-14}$  s $^{-1}$  (e.g., Indriolo et al. 2010; Le Petit et al. 2016). At these levels, the transformation

of CO into methanol and hydrocarbons proceeds much faster in the ice and gas, on scales of  $< 1$  Myr rather than 5–10 Myr (Bosman et al. 2018; Schwarz et al. 2018). Yet we still detect CO in some  $\lambda$  Orionis disks, and at levels expected from their millimeter continuum emission (Figure 4). However, the sample size of gas detections is small; deeper observations and additional molecular lines will help determine if our current CO nondetections are due to dispersal of the gas or chemical transformation of the CO.

Nevertheless, the massive stars in  $\lambda$  Orionis, through presupernova feedback and/or a recent supernova event itself, appear to have sculpted many of the observational features of the region yet have not significantly reduced the available planet-forming material in the overall disk population beyond what is expected at this evolved age.

## 6.2. External Photoevaporation in $\lambda$ Orionis

The OB stars can also impact the disk population through external photoevaporation (e.g., Johnstone et al. 1998; Störzer & Hollenbach 1999), a process that is now thought to be one of the main environmental factors depleting disk material (e.g., Scally & Clarke 2001; Sellek et al. 2020), even in typical galactic UV environments (e.g., Facchini et al. 2016; Haworth et al. 2016; Winter et al. 2018). While direct detection of externally driven photoevaporative winds is observationally challenging (Henney & O’Dell 1999; Rigliaco et al. 2009; Haworth & Owen 2020), indirect evidence based on the expected impacts on more easily observable disk properties is growing (e.g., Fang et al. 2012; Mann et al. 2014; Guarcello et al. 2016; Kim et al. 2016; Haworth et al. 2017; van Terwisga et al. 2019b). In particular, using ALMA to estimate disk masses, Ansdell et al. (2017) found in  $\sigma$  Orionis a dearth of massive ( $\gtrsim 1 M_{\text{Jup}}$ ) disks within  $\sim 0.5$  pc of the central OB stars, followed by a clear distance-dependent trend in disk mass out to the cluster edge (see their Figure 6).

Although we do not see a similar distance-dependent trend for the disk masses in  $\lambda$  Orionis, there is a lack of even low-mass ( $\gtrsim 0.1 M_{\text{Jup}}$ ) disks within  $\sim 0.3$  pc of the central OB stars (Figure 7) that could be a tentative signature of external photoevaporation (and/or ablation from the supernova; see Section 6.1). The lack of a distance-dependent trend in disk mass beyond 0.3 pc may be explained by the older age of the cluster, which has allowed for both more cluster expansion and dust grain growth. In this scenario, the sources in our sample were likely closer to the OB stars in the past, experiencing more effective external photoevaporation that removed gas and any entrained small dust grains in the outer disk. As the cluster dispersed with age, the remaining dust grains in the disks would have grown beyond 10–100  $\mu\text{m}$ , at which point they are too large to be affected by external photoevaporation and instead experience rapid inward radial drift (Haworth et al. 2018; Sellek et al. 2020). Thus, any detectable distance-dependent trend in disk mass may have been washed out due to the dynamical evolution of the cluster and the evolution of the disk dust population probed by ALMA for a couple Myr beyond the age of  $\sigma$  Orionis.

## 6.3. Outlier Disks in Evolved Regions

The handful of relatively nearby SFRs (at  $\lesssim 400$  pc; the distance of Orion or closer) with evolved ages ( $\sim 5$ –10 Myr old; the end of the disk lifetime) includes  $\lambda$  Orionis, Upper Sco, and

the TW Hya association (TWA). Each of these evolved regions contains at least one long-lived primordial disk that remains much more massive than the rest of the surviving disk population. Younger regions, in contrast, exhibit a smooth distribution in disk masses, regardless of whether they are in low-mass (e.g., Lupus) or high-mass (e.g., OMC-2) SFRs. This is illustrated in Figure 5, which shows the upper 32% of the disk dust mass distributions in different SFRs (32% was chosen to match the detection rate in our  $\lambda$  Orionis survey). In Figure 5, all of the SFRs exhibit similar slopes until the highest-mass disks, at which point the distributions of the evolved Upper Sco and  $\lambda$  Orionis regions rise steeply due to their outlier disks (we do not show TWA in Figure 5, as ALMA surveys of its disk population are not yet published). Additionally, the most massive disks in each SFR, regardless of age or environment, all have  $M_{\text{dust}} \sim 100 M_{\oplus}$ , which suggests that the outlier disks in the evolved regions were not distinct from birth but rather that some mechanism stopped the otherwise natural removal of disk material (e.g., by accretion onto the star and/or winds) as the disks evolved.

A potential explanation is that one or more (sub)stellar companions formed in these disks on orbits that are inhibiting the dispersal of outer disk material while also avoiding disk truncation/disruption, resulting in particularly long-lived primordial disks. A single massive super-Jupiter on an initially circular orbit may excite its own eccentricity (e.g., D’Angelo et al. 2006), enabling the clearing of a large inner cavity while preserving the outer disk; this has been demonstrated for the  $\sim 5$  Myr old PDS 70 system (Muley et al. 2019), which hosts a super-Jupiter planet at 22 au, and could potentially explain many other transition disks (van der Marel et al. 2018; van der Marel et al. 2020). Chains of gas giants (e.g., Zhu et al. 2011) and potentially super-Earths (Fung & Chiang 2017; Rosenthal et al. 2020) may also open inner disk cavities or large gaps. Although sufficiently inhibiting the accretion of gas-rich disk material (onto either the star or planets) to prolong disk lifetimes remains a challenge in these scenarios, dust evolution models show that giant planets drive strong pressure bumps that effectively prevent millimeter dust from drifting inward; these particle traps then result in prolonged lifetimes for the millimeter dust disks observed by ALMA, especially for higher-mass disks around higher-mass stars (e.g., Pinilla et al. 2020). Stellar binaries can also exert torques on disks that similarly open central cavities while also effectively inhibiting accretion of material onto the binary. Alexander (2012) showed that binaries on sufficiently close ( $\lesssim 1$  au) orbits form cavities smaller than the critical radius beyond which photoevaporative winds are efficient, resulting in circumbinary disk lifetimes that are several times longer than those of single-star disks. With these constraints in mind, we discuss below how the outlier disks in  $\lambda$  Orionis, Upper Sco, and TWA show evidence of such companions that could explain their extended primordial disk lifetimes.

For HD 245185 in  $\lambda$  Orionis, Kama et al. (2015) placed it in the population of Herbig Ae/Be stars whose stellar abundances are depleted in refractory elements while hosting warm/flared transition disks, as opposed to the population with solar abundances hosting cold/flat full disks. They explained the chemical peculiarity of the former population with giant planets filtering out dusty material as it flows through the disk, resulting in the accretion of high gas-to-dust ratio material onto

the star. These massive planets would then also be responsible for clearing out the large gap or cavity in the disk dust structure that defines the transition disk classification (Espaillat et al. 2014). Although our ALMA observations do not resolve any gaps or cavities in the disk around HD 245185 (Figure 3), the resolution is poor ( $\sim 60$  au in radius). As the SED of HD 245185 exhibits a mid-infrared dip (Ansdell et al. 2015), future ALMA observations may still resolve structure in the disk.

For Upper Sco, one of the most massive disks is around 2MASS J16042165–2130284 (also known simply as J1604), a negligible accretor (Manara et al. 2020) of K2 SpT that hosts a face-on transition disk with a large inner cavity seen in millimeter emission (Mathews et al. 2012; Ansdell et al. 2020). Evidence points to one or more high-mass planetary companions clearing out the cavity, as well as misaligning an unseen inner disk component that casts variable shadows on the outer disk detected in scattered light (e.g., Takami et al. 2014; Pinilla et al. 2018). This misaligned inner disk is also thought to cause the “dipper” variability observed in space-based light curves (e.g., Cody & Hillenbrand 2018; Ansdell et al. 2020). Another outlier disk in Upper Sco is around the G-type star 2MASS J15583692–2257153 (or HD 143006), which also hosts a face-on transition disk exhibiting “dipper” variability (Ansdell et al. 2020). This disk has a large gap, several narrow rings/gaps, and a bright asymmetry resolved by ALMA (Andrews et al. 2018b), suggesting a warped inner disk driven by a low-mass stellar or high-mass planetary companion potentially orbiting at a few au (Pérez et al. 2018). Finally, the most massive disk in Upper Sco is around 2MASS J16113134–1838259 (or AS 205); this is not a transition disk but displays clear spiral arms detected by ALMA, indicative of strong dynamical interactions induced by a known external companion (Kurtovic et al. 2018) that may be dominating its disk structure and evolution.

The outlier disk in TWA is around TW Hya itself. It also has an inner disk warp, this time detected in the gas kinematics (Rosenfeld et al. 2012), which could originate from a massive planetary companion orbiting this K-type star (e.g., Facchini et al. 2014). Extremely high-resolution ALMA observations have detected a gap at just 1 au, providing further evidence for interactions between the disk and a young planet (Andrews et al. 2016). Moreover, scattered-light images taken over nearly two decades show that an azimuthal asymmetry in the outer disk changes in P.A. in a manner consistent with shadowing by a precessing warped inner disk due to perturbations by a roughly Jupiter-mass companion orbiting at 1 au (Debes et al. 2017).

If some or all of these outlier disks are indeed due to substellar companions, they suggest that planet formation, given certain orbital parameters and mass ranges, can change the course of disk evolution to extend the lifetimes of primordial outer disks. More detailed analysis of these and other outlier disks—such as those in the older Upper Cen and Lower Cen regions (e.g., HD 142527, HD 135344B, HD 100453, and HD 100546)—could therefore provide insight into the timing and nature of planet formation. For now, we can only make some initial speculations. For example, early giant planet formation (occurring at  $\lesssim 1$  Myr) could help explain the outlier disks, as well as the apparent discrepancy between the amount of mass in protoplanetary disks compared to mature

exoplanet systems (Greaves & Rice 2010; Williams 2012; Najita & Kenyon 2014; Manara et al. 2018a). We note that observing one or two outlier disks within a given SFR, which typically hosts  $\sim 50$ – $100$  protoplanetary disks, is broadly consistent with the low occurrence rate of giant planets (e.g., Cumming et al. 2008; Bowler 2016; Nielsen et al. 2019), given that particularly massive or multiple gas giants and/or certain orbital parameters are likely required to create outlier disks. If the outlier disks are instead associated with the much more common compact multiplanet systems (e.g., Winn & Fabrycky 2015), this could suggest that such systems usually form in the outer disk and migrate inward, during which they disperse the outer disk; only in rarer cases do they form in situ, preserving the outer regions and resulting in an outlier disk.

## 7. Summary

We present an ALMA Band 6 survey of the protoplanetary disk population in the  $\lambda$  Orionis OB cluster. This region is important for studying disk evolution and planet formation due to its evolved age and the recent supernova that may have occurred in its core. Our key findings are as follows.

1. The millimeter emission from  $\lambda$  Orionis disks is weak but not particularly unusual given the cluster’s evolved age of  $\sim 5$  Myr. Only 14 of the 44 disks in our sample are detected in our observations of the 1.25 mm continuum (Figure 2), which has a  $34 \mu\text{Jy}$  median rms corresponding to  $3\sigma$  dust mass upper limits of  $\sim 0.4 M_{\oplus}$ . Stacking the 30 nondetections gives a  $4\sigma$  mean signal of  $20 \mu\text{Jy}$  ( $\sim 0.08 M_{\oplus}$ ), indicating that deeper observations should produce more detections. Only five disks are also detected in the  $^{12}\text{CO}$  line (Figure 3); however, the lack of gas detections is consistent with the weak continuum emission, based on the correlation between millimeter continuum and  $^{12}\text{CO}$  emission seen in younger regions (Figure 4).
2. The effects of massive stars, in the form of presupernova feedback and/or a supernova event itself, do not appear to significantly reduce the overall planet-forming capacity of a population of protoplanetary disks that is already a few Myr into evolution. This is based on comparing the disk mass distribution in  $\lambda$  Orionis to that of other SFRs, in particular the similarly aged Upper Sco association (Figures 5 and 6). One explanation is that supernovae are only effective at stripping mass from nearby disks that are within a small fraction of a parsec. Additionally, presupernova feedback may sculpt low-density channels in the intercluster gas through which energy can more easily escape, significantly muting the impact of supernova events on the surrounding disk population. However, more work is needed to confirm the occurrence of the supernova event in  $\lambda$  Orionis and/or determine whether a recent supernova also occurred in Upper Sco.
3. Massive “outlier” disks lingering in evolved ( $\sim 5$ – $10$  Myr) regions like  $\lambda$  Orionis, Upper Sco, and TWA show evidence for one or more (sub)stellar companions. Because these massive disks would not be considered outliers in younger ( $\sim 1$ – $2$  Myr) regions (Figure 5), their existence suggests that companion formation, including planet formation within certain orbital and mass constraints, can change the course of

disk evolution to extend the lifetimes of primordial outer disks. Further study of outlier disks as a population may therefore provide needed insight into the nature and timing of certain types of planet formation.

Many avenues for future work exist. Deeper ALMA observations of the disk population in  $\lambda$  Orionis will build up larger numbers of continuum and line detections to improve our constraints on population-level statistics. Understanding the disk population of the cluster members outside of the Spitzer survey area will also ensure that the ALMA survey is complete. Obtaining better constraints on the stellar and accretion properties of the disk-hosting stars in  $\lambda$  Orionis with wide-band and/or high-resolution spectra will allow us to search for trends seen in other regions, as well as any evidence for external photoevaporation and viscous evolution. Deeper observations with ALMA of multiple molecular lines tracing the gas content and chemistry will help determine whether our observations reflect disk gas dispersal or the transformation of CO due to enhanced cosmic-ray ionization from the supernova. Detailed theoretical studies may also provide insight into the peculiar kinematics of  $\lambda$  Orionis and its links to the star formation history of the region; similar studies in Upper Sco are also important, in particular to assess the possibility of a recent supernova having also occurred in that region. Indeed,  $\lambda$  Orionis still has much to teach us about perhaps one of the most common types of planet-forming environments in the nearby Galaxy.

M.A. and E.C. acknowledge support from NASA grant NNH18ZDA001N/EW. T.J.H. is funded by a Royal Society Dorothy Hodgkin Fellowship. This project has received funding from the European Union’s Horizon 2020 research and innovation program under Marie Skłodowska-Curie grant agreement No. 823823 (DUSTBUSTERS). This work was partly supported by the Deutsche Forschungs-Gemeinschaft (DFG; German Research Foundation), ref. No. FOR 2634/1 TE 1024/1-1. This work makes use of the following ALMA data: ADS/JAO.ALMA#2017.1.00466.S and #2016.1.00447.S. ALMA is a partnership of the ESO (representing its member states), NSF (USA), and NINS (Japan), together with the NRC (Canada), MOST and ASIAA (Taiwan), and KASI (Republic of Korea), in cooperation with the Republic of Chile. The Joint ALMA Observatory is operated by the ESO, AUI/NRAO, and NAOJ. This work made use of data from the European Space Agency (ESA) mission Gaia (<https://www.cosmos.esa.int/gaia>), processed by the Gaia Data Processing and Analysis Consortium (DPAC; <https://www.cosmos.esa.int/web/gaia/dpac/consortium>). Funding for the DPAC has been provided by national institutions, in particular the institutions participating in the Gaia Multilateral Agreement.

*Facilities:* ALMA, Gaia.

*Software:* *astropy* (Astropy Collaboration et al. 2013, 2018), *ASURV* (Lavalley et al. 1992), *CASA* (McMullin et al. 2007), *matplotlib* (Hunter 2007).

## Appendix A ALMA Observing Log

Table 3 summarizes the 13 execution blocks that collected the ALMA observations of our  $\lambda$  Orionis disk sample (Section 4.1). It provides the date and time of the observations

**Table 3**  
ALMA Observing Log

UTC Date (End Time)	$N_{\text{ant}}$	$L_{\text{base}}$ (m)	PWV (mm)	Calibrators (Bandpass/Flux, Phase)
2018-09-09 (13:39:36)	44	15–1213	2.1	J0423–0120, J0532+0732
2018-09-09 (10:58:12)	46	15–1213	1.7	J0510+1800, J0532+0732
2018-09-08 (13:09:24)	43	15–784	1.3	J0510+1800, J0532+0732
2018-09-01 (12:28:28)	45	15–784	1.7	J0510+1800, J0532+0732
2018-08-30 (12:15:34)	46	15–784	0.8	J0510+1800, J0532+0732
2018-01-24 (04:01:52)	44	15–1398	1.4	J0510+1800, J0532+0732
2018-01-23 (03:33:37)	43	15–1398	0.9	J0510+1800, J0532+0732
2018-01-22 (04:09:53)	44	15–1398	0.7	J0510+1800, J0532+0732
2018-01-22 (03:00:38)	44	15–1398	1.0	J0510+1800, J0532+0732
2018-01-21 (04:12:04)	44	15–1398	1.1	J0510+1800, J0532+0732
2018-01-21 (03:03:10)	44	15–1398	1.5	J0510+1800, J0532+0732
2018-01-19 (03:44:18)	45	15–1398	2.4	J0510+1800, J0532+0732
2018-01-18 (03:59:12)	44	15–1398	1.7	J0510+1800, J0532+0732

in Coordinated Universal Time (UTC Date), number of antennas used ( $N_{\text{ant}}$ ) and their baseline range ( $L_{\text{base}}$ ), precipitable water vapor (PWV) at the time of the observations, and names of the bandpass, flux, and gain calibrators applied in the pipeline calibration.

### Appendix B ALMA $^{12}\text{CO}$ Spectra

Figure 8 presents the ALMA Band 6  $^{12}\text{CO}$  spectra for all 44 sources in our  $\lambda$  Orionis disk sample. Extraction of the spectra is described in Section 4.3.

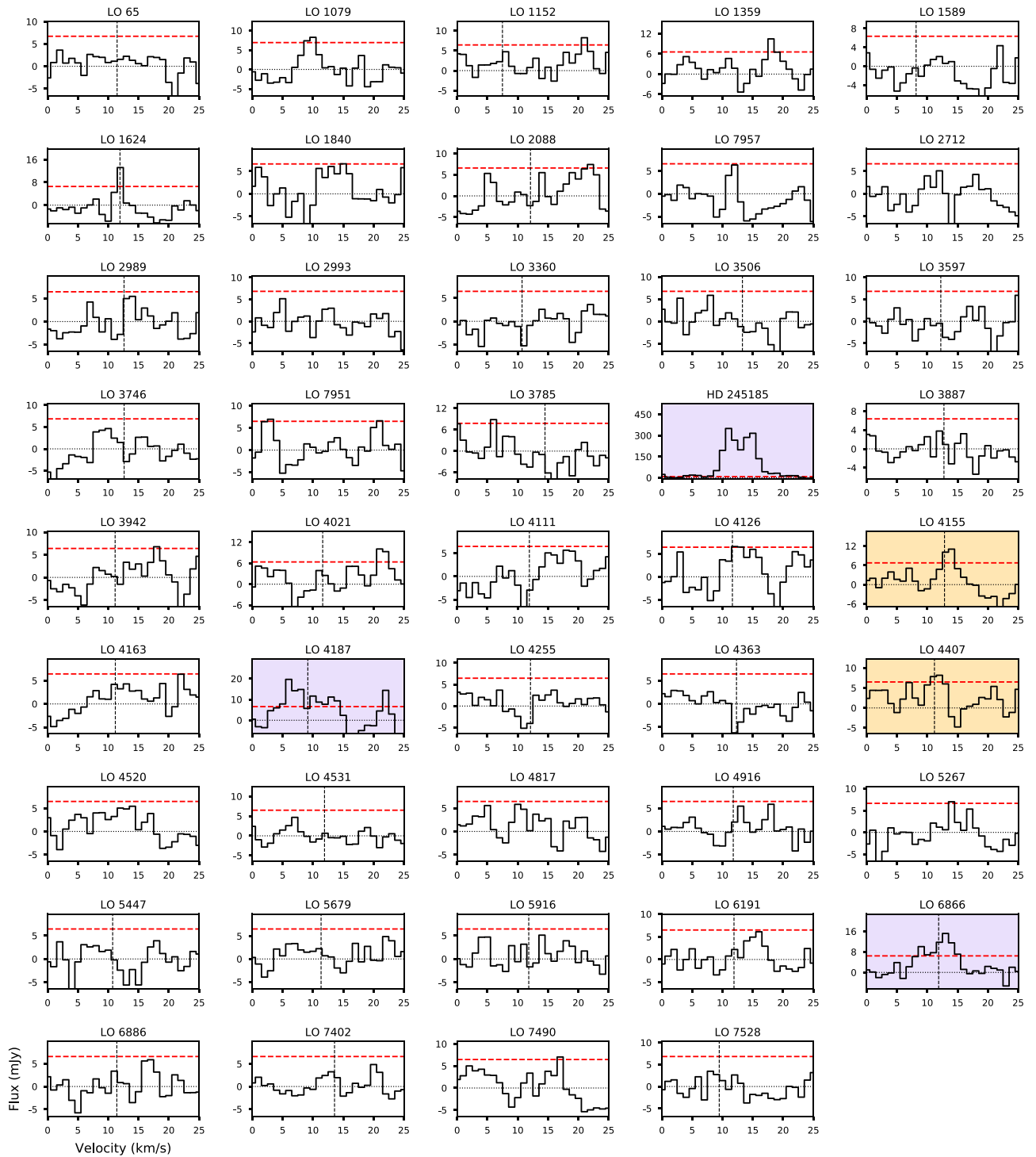


**Figure 8.** ALMA Band 6  $^{12}\text{CO}$  spectra for  $\lambda$  Orionis disks. Horizontal dashed red lines indicate  $3\times$  the median channel rms, while horizontal dotted black lines indicate the zero flux level. Vertical dashed lines are the source  $v_{\text{LSR}}$ , when available (Table 1). Clear detections ( $>4\sigma$ ) are highlighted in purple, while marginal detections ( $\sim 3\sigma\text{--}4\sigma$ ) are indicated with orange.

### ORCID iDs

Megan Ansdell <https://orcid.org/0000-0003-4142-9842>  
 Thomas J. Haworth <https://orcid.org/0000-0002-9593-7618>  
 Jonathan P. Williams <https://orcid.org/0000-0001-5058-695X>  
 Stefano Facchini <https://orcid.org/0000-0003-4689-2684>  
 Andrew Winter <https://orcid.org/0000-0002-7501-9801>  
 Carlo F. Manara <https://orcid.org/0000-0003-3562-262X>  
 Eugene Chiang <https://orcid.org/0000-0002-6246-2310>

Nienke van der Marel <https://orcid.org/0000-0003-2458-9756>  
 Ewine F. van Dishoeck <https://orcid.org/0000-0001-7591-1907>

### References

Adams, F. C. 2010, *ARA&A*, 48, 47  
 Alecian, E., Wade, G. A., Catala, C., et al. 2013, *MNRAS*, 429, 1027  
 Alexander, R. 2012, *ApJL*, 757, L29  
 Andrews, S. M. 2015, *PASP*, 127, 961

- Andrews, S. M. 2020, arXiv:2001.05007
- Andrews, S. M., Huang, J., Pérez, L. M., et al. 2018b, *ApJL*, **869**, L41
- Andrews, S. M., Rosenfeld, K. A., Kraus, A. L., & Wilner, D. J. 2013, *ApJ*, **771**, 129
- Andrews, S. M., Terrell, M., Tripathi, A., et al. 2018a, *ApJ*, **865**, 157
- Andrews, S. M., & Williams, J. P. 2005, *ApJ*, **631**, 1134
- Andrews, S. M., Wilner, D. J., Zhu, Z., et al. 2016, *ApJL*, **820**, L40
- Ansdell, M., Gaidos, E., Hedges, C., et al. 2020, *MNRAS*, **492**, 572
- Ansdell, M., Williams, J. P., & Cieza, L. A. 2015, *ApJ*, **806**, 221
- Ansdell, M., Williams, J. P., Manara, C. F., et al. 2017, *AJ*, **153**, 240
- Ansdell, M., Williams, J. P., Trapman, L., et al. 2018, *ApJ*, **859**, 21
- Ansdell, M., Williams, J. P., van der Marel, N., et al. 2016, *ApJ*, **828**, 46
- Astropy Collaboration, Price-Whelan, A. M., Sipőcz, B. M., et al. 2018, *AJ*, **156**, 18
- Astropy Collaboration, Robitaille, T. P., Tollerud, E. J., et al. 2013, *A&A*, **558**, A33
- Bailer-Jones, C. A. L., Rybizki, J., Fousneau, M., Mantelet, G., & Andrae, R. 2018, *AJ*, **156**, 58
- Baraffe, I., Homeier, D., Allard, F., & Chabrier, G. 2015, *A&A*, **577**, A42
- Barenfeld, S. A., Carpenter, J. M., Ricci, L., & Isella, A. 2016, *ApJ*, **827**, 142
- Bayo, A., Barrado, D., Stauffer, J., et al. 2011, *A&A*, **536**, A63
- Beckwith, S. V. W., Sargent, A. I., Chini, R. S., & Guesten, R. 1990, *AJ*, **99**, 924
- Bell, C. P. M., Naylor, T., Mayne, N. J., Jeffries, R. D., & Littlefair, S. P. 2013, *MNRAS*, **434**, 806
- Booth, A. S., & Ilee, J. D. 2020, *MNRAS*, **493**, L108
- Bosman, A. D., Walsh, C., & van Dishoeck, E. F. 2018, *A&A*, **618**, A182
- Ribas, Á., Bouy, H., & Merín, B. 2015, *A&A*, **576**, A52
- Bowler, B. P. 2016, *PASP*, **128**, 102001
- Cazzoletti, P., Manara, C. F., Baobab Liu, H., et al. 2019, *A&A*, **626**, A11
- Cieza, L. A., Ruiz-Rodríguez, D., Hales, A., et al. 2019, *MNRAS*, **482**, 698
- Clarke, C. J. 2007, *MNRAS*, **376**, 1350
- Cleeves, L. I., Bergin, E. A., & Adams, F. C. 2014, *ApJ*, **794**, 123
- Close, J. L., & Pittard, J. M. 2017, *MNRAS*, **469**, 1117
- Cody, A. M., & Hillenbrand, L. A. 2018, *AJ*, **156**, 71
- Concha-Márquez, F., Wilhelm, M. J. C., Portegies Zwart, S., & Haworth, T. J. 2019, *MNRAS*, **490**, 5678
- Cumming, A., Butler, R. P., Marcy, G. W., et al. 2008, *PASP*, **120**, 531
- Cunha, K., & Smith, V. V. 1996, *A&A*, **309**, 892
- Dale, J. E., Ngoumou, J., Ercolano, B., & Bonnell, I. A. 2014, *MNRAS*, **442**, 694
- D'Angelo, G., Lubow, S. H., & Bate, M. R. 2006, *ApJ*, **652**, 1698
- Davidson-Pilon, C., Kaldersam, J., Jacobson, N., et al. 2020, [CamDavidsonPilon/lifelines: v0.24.15, v0.24.15, Zenodo, doi:10.5281/zenodo.3934629](https://doi.org/10.5281/zenodo.3934629)
- de Geus, E. J. 1992, *A&A*, **262**, 258
- Debes, J. H., Poteet, C. A., Jang-Condell, H., et al. 2017, *ApJ*, **835**, 205
- Diplas, A., & Savage, B. D. 1994, *ApJS*, **93**, 211
- Dolan, C. J., & Mathieu, R. D. 1999, *AJ*, **118**, 2409
- Dolan, C. J., & Mathieu, R. D. 2001, *AJ*, **121**, 2124
- Eistrup, C., Walsh, C., & van Dishoeck, E. F. 2016, *A&A*, **595**, A83
- Espaillet, C., Muzerolle, J., Najita, J., et al. 2014, in *Protostars and Planets VI*, ed. H. Beuther et al. (Tucson, AZ: Univ. Arizona Press), 497
- Facchini, S., Clarke, C. J., & Bisbas, T. G. 2016, *MNRAS*, **457**, 3593
- Facchini, S., Ricci, L., & Lodato, G. 2014, *MNRAS*, **442**, 3700
- Fang, M., van Boekel, R., King, R. R., et al. 2012, *A&A*, **539**, A119
- Fazio, G. G., Hora, J. L., Allen, L. E., et al. 2004, *ApJS*, **154**, 10
- Folsom, C. P., Bagnulo, S., Wade, G. A., et al. 2012, *MNRAS*, **422**, 2072
- Fung, J., & Chiang, E. 2017, *ApJ*, **839**, 100
- Gaia Collaboration, Brown, A. G. A., Vallenari, A., et al. 2018, *A&A*, **616**, A1
- Gaia Collaboration, Prusti, T., de Bruijne, J. H. J., et al. 2016, *A&A*, **595**, A1
- Galli, P. A. B., Bouy, H., Olivares, J., et al. 2020, *A&A*, **634**, A98
- Greaves, J. S., & Rice, W. K. M. 2010, *MNRAS*, **407**, 1981
- Grénier, I. A., Black, J. H., & Strong, A. W. 2015, *ARA&A*, **53**, 199
- Guarcello, M. G., Drake, J. J., Wright, N. J., et al. 2016, arXiv:1605.01773
- Haworth, T. J., Boubert, D., Facchini, S., Bisbas, T. G., & Clarke, C. J. 2016, *MNRAS*, **463**, 3616
- Haworth, T. J., Facchini, S., Clarke, C. J., & Cleeves, L. I. 2017, *MNRAS*, **468**, L108
- Haworth, T. J., Facchini, S., Clarke, C. J., & Mohanty, S. 2018, *MNRAS*, **475**, 5460
- Haworth, T. J., & Owen, J. E. 2020, *MNRAS*, **492**, 5030
- Henney, W. J., & O'Dell, C. R. 1999, *AJ*, **118**, 2350
- Herczeg, G. J., & Hillenbrand, L. A. 2015, *ApJ*, **808**, 23
- Hernández, J., Calvet, N., Briceño, C., et al. 2007, *ApJ*, **671**, 1784
- Hernández, J., Calvet, N., Hartmann, L., et al. 2009, *ApJ*, **707**, 705
- Hernández, J., Morales-Calderon, M., Calvet, N., et al. 2010, *ApJ*, **722**, 1226
- Hildebrand, R. H. 1983, *QJRAS*, **24**, 267
- Hollenbach, D., Johnstone, D., Lizano, S., & Shu, F. 1994, *ApJ*, **428**, 654
- Hoogerwerf, R., de Bruijne, J. H. J., & de Zeeuw, P. T. 2000, *ApJL*, **544**, L133
- Hoogerwerf, R., de Bruijne, J. H. J., & de Zeeuw, P. T. 2001, *A&A*, **365**, 49
- Hunter, J. D. 2007, *CSE*, **9**, 90
- Indriolo, N., Blake, G. A., Goto, M., et al. 2010, *ApJ*, **724**, 1357
- Johnstone, D., Hollenbach, D., & Bally, J. 1998, *ApJ*, **499**, 758
- Kama, M., Folsom, C. P., & Pinilla, P. 2015, *A&A*, **582**, L10
- Kenyon, S. J., & Hartmann, L. 1995, *ApJS*, **101**, 117
- Kim, J. S., Clarke, C. J., Fang, M., & Facchini, S. 2016, *ApJL*, **826**, L15
- Kounkel, M., Covey, K., Suárez, G., et al. 2018, *AJ*, **156**, 84
- Kurtovic, N. T., Pérez, L. M., Benisty, M., et al. 2018, *ApJL*, **869**, L44
- Lang, W. J., Masheder, M. R. W., Dame, T. M., & Thaddeus, P. 2000, *A&A*, **357**, 1001
- Lavalley, M., Isobe, T., & Feigelson, E. 1992, in *ASP Conf. Ser.*, **25**, ASURV: Astronomy Survival Analysis Package, ed. D. M. Worrall, C. Biemesderfer, & J. Barnes (San Francisco, CA: ASP), 245
- Le Petit, F., Ruaud, M., Bron, E., et al. 2016, *A&A*, **585**, A105
- Lee, D., Seon, K.-I., & Jo, Y.-S. 2015, *ApJ*, **806**, 274
- Lucas, W. E., Bonnell, I. A., & Dale, J. E. 2020, *MNRAS*, **493**, 4700
- Luhman, K. L., & Esplin, T. L. 2020, *AJ*, **160**, 44
- Lynden-Bell, D., & Pringle, J. E. 1974, *MNRAS*, **168**, 603
- Maddalena, R. J., & Morris, M. 1987, *ApJ*, **323**, 179
- Majewski, S. R., Schiavon, R. P., Frinchaboy, P. M., et al. 2017, *AJ*, **154**, 94
- Manara, C. F., Morbidelli, A., & Guillot, T. 2018a, *A&A*, **618**, L3
- Manara, C. F., Natta, A., Rosotti, G. P., et al. 2020, *A&A*, **639**, A58
- Manara, C. F., Prusti, T., Comeron, F., et al. 2018b, *A&A*, **615**, L1
- Mann, R. K., Di Francesco, J., Johnstone, D., et al. 2014, *ApJ*, **784**, 82
- Mathews, G. S., Williams, J. P., & Ménard, F. 2012, *ApJ*, **753**, 59
- Mathieu, R. 2015, in *Dynamics of Young Star Clusters and Associations*. Saas-Fee Advanced Course, Vol. 42, ed. M. Meyer, L. Eyer, & C. Bell (Berlin: Springer), 147
- Mathieu, R. D. 2008, in *Handbook of Star Forming Regions*, Vol. I, ed. B. Reipurth (San Francisco, CA: ASP), 757
- Maxted, P. F. L., Jeffries, R. D., Oliveira, J. M., Naylor, T., & Jackson, R. J. 2008, *MNRAS*, **385**, 2210
- McMullin, J. P., Waters, B., Schiebel, D., Young, W., & Golap, K. 2007, in *ASP Conf. Ser.*, **376**, *CASA Architecture and Applications*, ed. R. A. Shaw, F. Hill, & D. J. Bell (San Francisco, CA: ASP), 127
- Miotello, A., Facchini, S., van Dishoeck, E. F., et al. 2019, *A&A*, **631**, A69
- Miotello, A., van Dishoeck, E. F., Williams, J. P., et al. 2017, *A&A*, **599**, A113
- Muley, D., Fung, J., & van der Marel, N. 2019, *ApJL*, **879**, L2
- Murdin, P., & Penston, M. V. 1977, *MNRAS*, **181**, 657
- Najita, J. R., & Kenyon, S. J. 2014, *MNRAS*, **445**, 3315
- Nielsen, E. L., De Rosa, R. J., Macintosh, B., et al. 2019, *AJ*, **158**, 13
- Pascucci, I., Testi, L., Herczeg, G. J., et al. 2016, *ApJ*, **831**, 125
- Pérez, L. M., Benisty, M., Andrews, S. M., et al. 2018, *ApJL*, **869**, L50
- Pinilla, P., Benisty, M., de Boer, J., et al. 2018, *ApJ*, **868**, 85
- Pinilla, P., Pascucci, I., & Marino, S. 2020, *A&A*, **635**, A105
- Rieke, G. H., Young, E. T., Engelbracht, C. W., et al. 2004, *ApJS*, **154**, 25
- Rigliaco, E., Natta, A., Randich, S., & Sacco, G. 2009, *A&A*, **495**, L13
- Rosenfeld, K. A., Qi, C., Andrews, S. M., et al. 2012, *ApJ*, **757**, 129
- Rosenthal, M. M., Chiang, E. I., Ginzburg, S., & Murray-Clay, R. A. 2020, *MNRAS*, **498**, 2054
- Sacco, G. G., Franciosini, E., Randich, S., & Pallavicini, R. 2008, *A&A*, **488**, 167
- Scally, A., & Clarke, C. 2001, *MNRAS*, **325**, 449
- Schwarz, K. R., Bergin, E. A., Cleeves, L. I., et al. 2018, *ApJ*, **856**, 85
- Sellek, A. D., Booth, R. A., & Clarke, C. J. 2020, *MNRAS*, **492**, 1279
- Siess, L., Dufour, E., & Forestini, M. 2000, *A&A*, **358**, 593
- Skrutskie, M. F., Cutri, R. M., Stiening, R., et al. 2006, *AJ*, **131**, 1163
- Störzer, H., & Hollenbach, D. 1999, *ApJ*, **515**, 669
- Takami, M., Hasegawa, Y., Muto, T., et al. 2014, *ApJ*, **795**, 71
- Tazzari, M., Testi, L., Natta, A., et al. 2017, *A&A*, **606**, A88
- Trapman, L., Ansdell, M., Hogerheijde, M. R., et al. 2020, *A&A*, **638**, A38
- Tripathi, A., Andrews, S. M., Birnstiel, T., & Wilner, D. J. 2017, *ApJ*, **845**, 44
- van der Marel, N., Birnstiel, T., Garufi, A., et al. 2020, arXiv:2010.10568
- van der Marel, N., Williams, J. P., Ansdell, M., et al. 2018, *ApJ*, **854**, 177
- van Terwisga, S. E., Hacar, A., & van Dishoeck, E. F. 2019a, *A&A*, **628**, A85
- van Terwisga, S. E., van Dishoeck, E. F., Cazzoletti, P., et al. 2019b, *A&A*, **623**, A150
- Williams, J. P. 2012, *M&PS*, **47**, 1915
- Winn, J. N., & Fabrycky, D. C. 2015, *ARA&A*, **53**, 409

- Winter, A. J., Clarke, C. J., Rosotti, G., et al. 2018, [MNRAS](#), **478**, 2700
- Winter, A. J., Clarke, C. J., & Rosotti, G. P. 2019, [MNRAS](#), **485**, 1489
- Winter, A. J., Kruijssen, J. M. D., Chevance, M., Keller, B. W., & Longmore, S. N. 2020, [MNRAS](#), **491**, 903
- Wyatt, M. C. 2008, [ARA&A](#), **46**, 339
- Zamora-Avilés, M., Ballesteros-Paredes, J., Hernández, J., et al. 2019, [MNRAS](#), **488**, 3406
- Zhu, Z., Nelson, R. P., Hartmann, L., Espaillat, C., & Calvet, N. 2011, [ApJ](#), **729**, 47
- Zhu, Z., Zhang, S., Jiang, Y.-F., et al. 2019, [ApJL](#), **877**, L18